1-1-2002

Calculation of array probe response to sub-surface corrosion using edge element

Vipul Katyal
Iowa State University

Calculation of array probe response to sub-surface corrosion using edge element

by

Vipul Katyal

A thesis submitted to the graduate faculty

in partial fulfillment of the requirements for the degree of

MASTER OF SCIENCE

Major: Electrical Engineering

Program of Study Committee:
John R. Bowler, Major Professor
Gary Tuttle
R. Bruce Thompson

Iowa State University

Ames, Iowa

2002

Graduate College
Iowa State University

This is to certify that the master's thesis of

Vipul Katyal

has met the thesis requirements of Iowa State University

Signatures have been redacted for privacy

DEDICATION

I would like to dedicate this thesis to my father, Dr. O. P. Katyal, an inspiring teacher of physics, and to my mother, Ms. M. Katyal, for their support and guidance without which I would not have been able to complete this work.

TABLE OF CONTENTS

LIST OF TABLES

LIST OF FIGURES

ABSTRACT

The area of non-destructive evaluation using eddy current methods is continuously evolving with the better understanding of the technique. In the past decade or so, new designs have emerged for excitation coils which has led to a need for new modelling schemes. There has been a trend towards the use of magnetic field sensors for the measurement of the scattered field from the conductor body as an alternative to induction coils. Along with the changes in the driver-pickup arrangement, there are changes in the area of computation methods of finding solutions to the forward and inverse problems. We need to have a good forward models for finding solutions to an inverse problem . Use of newer discretization schemes has led to better and faster models. In this thesis, I have examined two aspects of the problem of eddy current detection. The first part is devoted to the development of a new analysis of a racetrack coil used with an array of magnetic field sensors. The later part is dedicated to finding a numerical solution to the problem of the interaction of the excitation coil with a flaw. The solution uses edge element basis functions for the expansion of the unknown field in the flaw.

CHAPTER 1. OVERVIEW

Advances in the area of non-destructive evaluation (NDE) using eddy current methods have lead to an increase in there value to industry. These advances are related to the development of new coil designs, the use of magnetic sensors for the detection of the scattered field, the modelling of complex geometries using different meshing schemes and the development of improved methods for the solution of forward and inverse problem. These developments have lead to the better understanding of the technical details of eddy current problems. In the general eddy current problem, a coil or a magnetic field sensor, e.g. giant magneto-resistive sensor (GMR), amorphous magneto-resistive sensor (AMR), extraordinary magneto-resistive sensor (EMR), Hall sensor etc., detects field perturbations due to the variation of conductivity and permeability of an electrically conducting component. A crack or flaw is defined to be a region that does not conduct electricity. Hence it will perturb the surrounding field and cause a disturbance of the field which can be then sensed by the pick-up coil or probe or a magnetic field sensor. As the magnetic field sensors have a higher spatial resolution than the pick-up coils, they are more effective at imaging the flaw. This leads to a demand of the use of magnetic field sensors in the eddy current applications.

The other area of development in eddy current NDE is solving the inverse problem in which the characteristics of an actual physical flaw are found from flaw measurements. Usually this problem requires the solution of the forward problem first. In a forward problem we have a known flaw profile and try to estimate theoretically its interaction with an eddy current excitation coil. There are many different ways of solving a forward problem, e.g finite element method (FEM), integral equations (IE) etc.

Over the past years a lot of work on FEM has been carried out to achieve better numerical

modelling of different problems in electromagnetism. The FEM has been applied to scattering problems, material interface problems, eddy current problems and many more. A detailed discussion of the application of FEM in eddy current problems is presented by Albanese and Rubinacci, (2). They have proposed the solution of a problem based on the edge element formulation, whose degrees of freedom are associated with the tangential components of the vector field along the edges of volume elements, in conjunction with the tree-cotree decomposition of the discretizing mesh. They have first developed the mathematical model and then shown the application of the edge element based integral formulation for linear and nonlinear eddy current problems. A discussion on the benefits of using vector potentials with a gauge condition, e.g. classic Coulomb and Lorentz gauges, in dealing with eddy current problems, material interfaces and magnetostatic problems are also presented.

A similar treatment of computational methods in electromagnetism is presented in the book "Computational Electromagnetism" by Bossavit, (6), and "The Finite Element Method in Electromagnetics" by Jin, (24). Bossavit presented a mathematical analysis of edge elements in terms of Whitney elements and the application of tree-cotree decomposition is described for curl-free fields. Use of tree-cotree decomposition then guarantees a unique solution of the problem. Jin has presented a discussion on the application of FEM in waveguide and cavity problems. He has also looked at three dimensional edge elements for different discretization geometries and described FEM matrix solution methods using LU and LDL^T decomposition, and the conjugate gradient approach.

Another application of edge elements is for resonant cavities where the problem of spurious modes, which appears using conventional nodal elements, is avoided. Sun, Manges, Yuan and Cendes examined the spurious modes problem in their paper, (31). They have discussed the spurious modes problem in the solution of a vector wave equation which arises due to the inconsistent approximations of the static solutions to the wave equation. These modes are caused because of the incorrect approximation of the null space of the curl operator. In the paper they have presented the use of tangential-vector finite elements to ensure tangential continuity of the vector field and hence avoided the inconsistencies in the solution process.

Albanese and Rubinacci described an integral formulation of the eddy current problem using edge elements, (3). They presented the formulation based on the current vector potential approach, i.e. the current density is defined as a curl of a vector, which assures the solenoidality of current density. The gauge condition and the boundary conditions are directly imposed by the edge element shape functions and the methods of network theory. Based on this theory they have developed a FEM code employing an eight-node brick element structure. They have also compared integral and differential methods in an eddy current problem using a vector potential formulation, (4).

Integral equation formulations have also taken advantage of new developments in the type of basis functions for the expansion of the unknowns. Schaubert, Wilton and Glisson in their paper, (31), presented the use of tetrahedral modelling along with the use of special basis functions which ensure the normal continuity of the flux density across the faces of the tetrahedrons. This eliminates the problem of the divergence of the solution as compared to the case where pulse basis functions are used for expansion.

A similar analysis of basis functions is also presented by Graglia, Wilton and Peterson, (20). They have presented vector basis functions that are compatible with the curl-conforming and divergence-conforming mixed-order Nedelec spaces. Curl-conforming functions, which maintains only tangential continuity across the element boundaries, are helpful in modelling fields at the material boundaries and are able to suppress the spurious modes. They are appropriate for discretization of the vector Helmholtz operator. On the other hand, divergence-conforming functions maintain normal continuity across the element interface. They eliminate spurious solutions in the electric field integral equation (EFIE). Different discretization schemes, e.g. triangular, quadrilateral, tetrahedral, brick elements, and curvilinear, along with curl-conforming and divergence-conforming basis functions are described, (20).

The use of the EFIE for an eddy current problem of a surface crack has been presented by Bowler, Jenkins, H. Sabbagh and L. Sabbagh, (10). A change of coil impedance due to the scattered field of a volumetric flaw is determined. A volume integral equation with a dyadic kernel has been derived and the numerical solution is found by the use of the moment

method and the conjugate gradient approach. The theoretical results are then compared with experimental results. A detailed analysis of the calculation of the eddy current response using dyadic kernels is presented by Bowler, (9). In the report, both forward problems and inverse problems are addressed for an ideal crack problem. In addition, a detailed analysis of the EFIE approach using dyadic Green's function is giving for cracks in a half-space, slab and layered conductors. Rooftop basis functions are used for finding the solution numerically for the crack interaction problem. A detailed analysis on handling the singularity of the Green's function is also given. A similar approach for handling the singularity of the Green's function is presented by Lee, Boersma, Law and Deschamps, (26).

The use of edge element shape functions instead of rooftop functions in the EFIE eddy current problem has been presented by Rubinacci and Tamburrino, (30). They expanded the unknown current density in terms of the curl of the edge based shape function to ensure normal continuity across the surface of the discretization cell and hence will suppress spurious modes in the EFIE solution as describe by Graglia, Wilton and Peterson in (20).

With the above background, I have obtained solutions of an eddy current problem using the electric field integral equation based techniques. The two main topics presented here concern a new eddy current coil analysis for a racetrack coil to be used with an array of magnetic field sensors, Chapter 2, and in Chapter 3, a new discretization scheme for solving the EFIE using edge elements following the fromulation given in reference (30).

1.1 NEW COIL DEVELOPMENT FOR AN ARRAY OF MAGNETIC FIELD SENSORS

The advantages of a magnetic field sensor over a pick-up coil are describe earlier. A drawback of using a single sensor, whether it be a solid state sensor or a pick-up coil, is that a two dimensional scan is usually needed to cover a given area. That can be time consuming procedure. Therefore, the next step in the development process is to have a linear array of sensors. This will result in a rapid inspection as we can scan a larger area in fewer steps in one direction. Also we can multiplex the signals from all the sensors to a few or only one channel,

therefore achieving a cost effective and efficient solution. As we are moving towards the use of a linear array of sensors, the most effective shape for the excitation coil is a "racetrack" design, where we have two straight parts and two semicircular bends, Fig. 1.1. The sensors are aligned parallel to the straight parts of the coil, hence the field experienced by each sensor will similar yet the coil design is compact.

A magnetic shell model is used for finding the electric field response of the excitation coil, (8). The problem of calculating the coil field is then subdivided into two parts. In the first part, the electric field due to the straight parts only is found and in the second part, the electric field due to the semicircular bends is computed. To find the response of recess in a stratified conductor, two methods were used in which the EFIE is used to calculate the dipole density. This was accomplished using a dyadic form of the Green's function, (9) - (8), (33). The earlier method for handling of the singularity of the Green's function is given in (9), (26). Rooftop basis functions are used for expanding the unknown dipole density. The earlier EFIE is solved using Galerkin method for moment method, (9) with point matching scheme. Analysis of the new coil is validated by comparing the results of a limiting case of racetrack coil where the straight parts are set to zero to that of a circular coil results. The new method for finding the dipole density from the EFIE uses edge element basis function.

1.2 USE OF NEW BASIS FUNCTION FOR FINDING THE DIPOLE DENSITY

For finding the response of a crack or flaw interaction with a excitation coil, we need to solve for the unknown dipole density due to the excitation coil in the flaw region. This is solved using the EFIE method, as described earlier. One of the main property of the dipole density inside a homogeneous flaw is that it has zero divergence. This property is not guaranteed by using rooftop basis function, which are used earlier in the volume element scheme. A basis function that ensures the above property of zero divergence is the edge shaped basis function (2) - (3), (24), (30). By expanding the unknown dipole density as a curl of these new basis functions, i.e. forming a divergence-conforming basis, ensure the removal of spurious modes from the

EFIE solution set. The next step of development is to use tree-cotree decomposition, (2), (6), (30), which will eliminate dependent equations and hence we will have a unique solution to the problem along with better convergence. Using the new set of basis functions and tree-cotree decomposition, a set of matrix equations are formed for solving for the unknown dipole densities. An LU decomposition, (24) and (29), is used for solving the set of linear equations. A comparison is made between the results of the new technique with that of the point matching scheme.

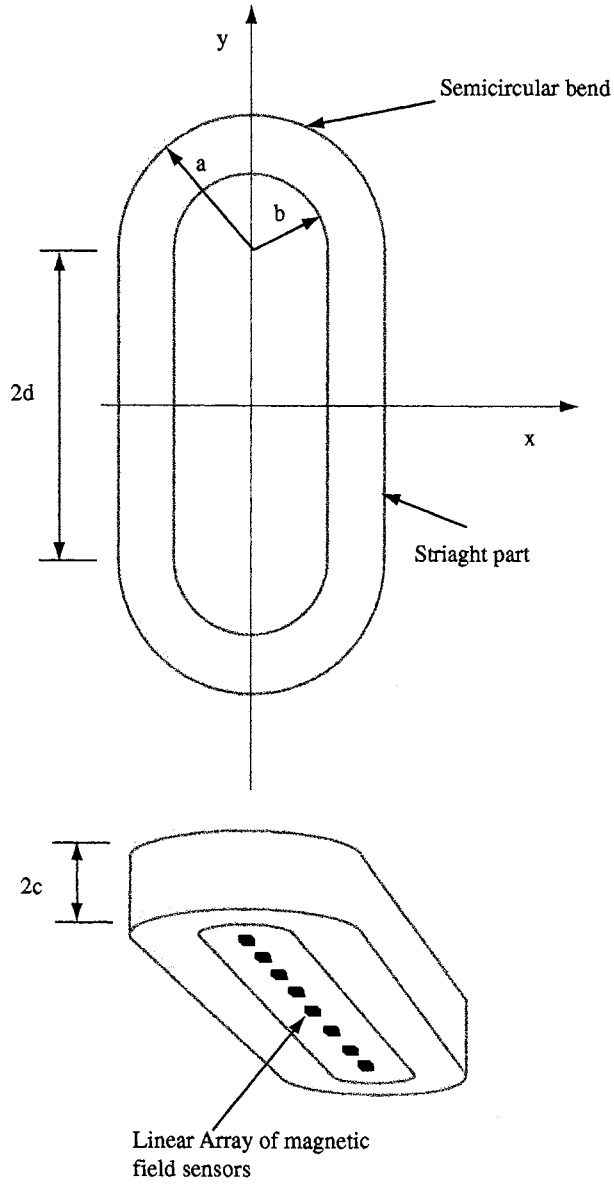

Figure 1.1 Racetrack probe geometry showing straight parts and semicircular bends along with linear array of magnetic field sensors.

CHAPTER 2. EDDY CURRENT EXCITATION USING A RACETRACK COIL WITH A SENSOR ARRAY FOR MAGNETIC FIELD MEASUREMENT

A paper to be submitted to the Journal of Applied Physics

J. R. Bowler [1] and V. Katyal [2]

ABSTRACT

Calculations have been performed to determine the response of a new eddy current probe for the detection of subsurface flaws in planar multilayered structures. The probe consists of a racetrack coil and a linear array of solid state sensors for detecting perturbations in the electromagnetic field due to defects. The sensor array allows field measurements to be made at a number of closely spaced locations without moving the probe and thereby accelerates the inspection process. A magnetic shell model of the probe is used for finding the electric field in the unflawed structure. The fields due to the linear "straights" and the semicircular "bends" are found separately and added to give the combined field of the racetrack coil. The flaw response is then computed using a volume element calculation. In order to validate the calculation, field predictions for a racetrack coil having straights of zero length are compared with results for a circular coil. The results are found to be consistent.

2.1 INTRODUCTION

In eddy current inspection, an induction coil is often used both to induce current in a conducting component and to detect magnetic field perturbations due to flaws. For subsurface

[1]Professor, Department of Electrical and Computer Engineering, Iowa State University
[2]Graduate Student, Department of Electrical and Computer Engineering, Iowa State University

defects, a low frequency excitation ensures an adequate depth of field penetration. However, at lower frequencies the effectiveness of the coil as both inducer and sensor is diminished since electromagnetic induction depends on the rate of change of magnetic flux. To overcome the limitations of the induction coil as a low frequency field sensor, a solid state device, such as a giant magneto-resistor or Hall sensor, can be used instead. A coil used only as driver can be larger than otherwise without compromising the spatial resolution of the measurements. The large coil can produce a greater field while good spatial resolution is obtained by using small sensors.

This article gives the analysis of an eddy current probe for the detection of subsurface flaws in multilayered structures such as aircraft skins. The probe contains a racetrack coil with semi-circular bends and linear straights, Fig. 2.1. The magnetic field between the straights is measured using a linear array of magnetic field sensors. The sensor array samples the magnetic field at multiple sites without moving the probe and hence reduces the inspection time. The overall objective of this work is to evaluate the capabilities of array probes and assess their performance for the detection of cracks, material loss and surface roughness due to corrosion. Here we focus on the details of the coil field calculation.

The theory for computing the electromagnetic field of a racetrack coil, Fig. 2.1, has been developed by determining separately the electric field due to the bends and the straights and summing to obtain the total field. Section II gives the theory for the straight linear coil elements and Section III describes the solution for the D-coil representing a semicircular bend. The results and conclusions follow the analysis sections.

2.2 LINEAR COIL FIELD

The following account describes the calculation of the electric field induced in a conductor by a time-harmonic current in a linear coil consisting of only the straight parts of the racetrack coil shown in Fig. 2.1. The current path is closed by joining the ends of the straights by current filaments but ultimately the effect of these filaments is cancelled by similar filaments added to the representation of the bends. Results are given for a field in a homogeneous half-

space conductor in the region $z < 0$, and an infinite conducting plate. However, similar results for layered conductors are readily obtained by simply changing the Green's functions used in the present calculation in favor of one which embodies the correct interface conditions of a stratified conductor. The magnetic dipole formulation used in this section to represent the field of the straights is also used for the bends in the next section.

Consider a non-magnetic conductor occupying the half-space defined by $z < 0$, excited by a current source. The electric field in adjoining half-spaces is a solenoidal solution of,

$$\nabla^2 \mathbf{E}(\mathbf{r}) = \jmath\omega\mu_0 \mathbf{J}(\mathbf{r}), \quad z \geq 0 \qquad \text{and} \qquad \left(\nabla^2 - \jmath\omega\mu_0\sigma\right)\mathbf{E}(\mathbf{r}) = 0, \quad z < 0, \tag{2.1}$$

where σ is the conductivity of the conductor. The electric field, being transverse to the $z-$direction and having zero divergence, can be expressed in terms of a transverse electric (TE), scalar potential:

$$\mathbf{E}(\mathbf{r}) = -\jmath\omega\mu\nabla \times \hat{z}\psi'(\mathbf{r}) \tag{2.2}$$

where $\hat{z}$ is a unit vector in the preferred direction. The transverse source current $\mathbf{J}(\mathbf{r})$, having zero divergence, can similarly be written in transverse scalar form as

$$\mathbf{J}(\mathbf{r}) = \frac{1}{\mu_0}\nabla \times [\hat{z}M(\mathbf{r})]. \tag{2.3}$$

The function $M(\mathbf{r})$ represents the current source in terms of the magnetic dipole density, the orientation of the polarization being in the $z-$direction. This is an adaptation of the magnetic shell model which represents a filamentary current loop in terms of magnetic shell bounded by the loop. Here, the magnetic dipole distribution occupies a volumetric region between the upper and lower extent of the coil where $h + c \geq z \geq h - c$, $2c$ being the height of the coil and h the height of the mid point of the coil above the surface of the conductor.

Equations (2.2) and (2.3) are substituted into (2.1) to give

$$\nabla^2\psi'(\mathbf{r}) = -\frac{1}{\mu_0}M(\mathbf{r}), \quad z \geq 0 \qquad \text{and} \qquad \left(\nabla^2 - \jmath\omega\mu_0\sigma\right)\psi'(\mathbf{r}) = 0, \quad z < 0. \tag{2.4}$$

An expression for the solution in terms of a Green's function, satisfying

$$\nabla^2 G(\mathbf{r}, \mathbf{r}') = -\delta(\mathbf{r} - \mathbf{r}'), \quad z \geq 0 \qquad \text{and} \qquad \left(\nabla^2 - \jmath\omega\mu_0\sigma\right)G(\mathbf{r}, \mathbf{r}') = 0, \quad z < 0, \tag{2.5}$$

is written as

$$\psi'(\mathbf{r}) = \frac{1}{\mu_0} \int_{\Omega_0} G(\mathbf{r}, \mathbf{r}')\, M(\mathbf{r}')\, d\mathbf{r}. \tag{2.6}$$

where the Green's function, like ψ', is continuous at the air conductor interface, has a continuous normal gradient and vanishes at infinity. The Fourier transform with respect to x and y is written

$$\widetilde{f}\,(u,v) = \int_{-\infty}^{\infty} \int_{-\infty}^{\infty} f(x,y) e^{-iux-ivy}\, dx\, dy. \tag{2.7}$$

Hence by taking the Fourier transform of equation (2.6) with respect to x and y, and noting the convolutional properties of the integral, it is found that

$$\widetilde{\psi}'\,(u,v,z) = \frac{1}{\mu_0} \int_{h-c}^{h+c} \widetilde{g}\,(u,v,z,z')\, \widetilde{m}\,(u,v,z')\, dz', \tag{2.8}$$

where the integration is between the lower and upper limits of the source coil and $\widetilde{g}$ and $\widetilde{m}$ are the Fourier transforms of G and M respectively.

The y-component of the current density in the straight elements of the source coil, Fig. 2.1, is written as

$$J_y(\mathbf{r}) = \begin{cases} nI\,\mathrm{sign}(x), & h-c \le z \le h+c, \quad b \le |x| \le a, \quad |y| \le d, \\ 0, & \text{otherwise} \end{cases} \tag{2.9}$$

where I is the current, n the number of turns per unit area and the current is deemed to flow in a counter-clockwise direction viewed from above. It can be deduced from (2.3), by writing

$$M(x,y,z) = \begin{cases} \mu_0 n I f(x,y), & h-c \le z \le h+c \\ 0, & \text{otherwise} \end{cases} \tag{2.10}$$

that

$$f(x,y) \;=\; \begin{cases} a-b, & 0 \le |x| \le b, \quad |y| \le d, \\ a-|x|, & b \le |x| \le a, \quad |y| \le d, \\ 0, & \text{otherwise.} \end{cases} \tag{2.11}$$

Because $f(x,y)$ is even in x and y, the Fourier transform may be written in the form of the double cosine integral

$$\begin{aligned} \widetilde{f}\,(u,v) &= 4 \int_0^{\infty} \int_0^{\infty} f(x,y) \cos(ux) \cos(vy)\, dx\, dy \\ &= -\frac{4}{u^2 v} \left[\cos(ua) - \cos(ub)\right] \sin(vd). \end{aligned} \tag{2.12}$$

An expression for the electric field which can be evaluated numerically is obtained in the following way. The Fourier transform of (2.2) with respect to x and y is

$$\widetilde{\mathbf{e}}\,(u,v,z) = -\omega\mu_0(v\hat{x} - u\hat{y})\;\widetilde{\psi'}\,(u,v,z) \tag{2.13}$$

where $\widetilde{\psi'}$ is given by (2.8) and (2.10) as

$$\widetilde{\psi'}\,(u,v,z) = nI\,\widetilde{f}\,(u,v)\int_{h-c}^{h+c}\widetilde{g}\,(u,v,z,z')\,dz', \qquad z<0. \tag{2.14}$$

For a half-space conductor

$$\widetilde{g}_{\text{H-S}}(\kappa,z,z') = \frac{1}{\gamma+\kappa}e^{\gamma z-\kappa z'} \tag{2.15}$$

where $\gamma = \sqrt{\kappa^2 + j\omega\mu_0\sigma}$, taking the root with a positive real part. Similarly, Green's function for a slab is computed by taking into account the reflection from the internal surfaces,

$$\widetilde{g}_{\text{Slab}}(\kappa,z,z') = \frac{1}{\gamma+\kappa}e^{\gamma z-\kappa z'}\frac{1+\Gamma e^{-2\gamma(d+z)}}{1-\Gamma^2 e^{-2\gamma d}} \tag{2.16}$$

where $\Gamma = \frac{\gamma-\kappa}{\gamma+\kappa}$, the reflection term and d = height of the slab. Performing the integration in (2.14) gives

$$\widetilde{\psi'}\,(u,v,z) = 2nI\,\widetilde{f}\,(u,v)\,\widetilde{g}\,(u,v,z,h)\sinh(\kappa c)/\kappa, \qquad z<0, \tag{2.17}$$

hence by substituting into (2.13) it is found that

$$\widetilde{\mathbf{e}}\,(u,v,z) = -2\omega\mu_0 nI\frac{v\hat{x}-u\hat{y}}{\kappa}\;\widetilde{f}\,(u,v)\,\widetilde{g}\,(u,v,z,h)\sinh(\kappa c), \qquad z<0. \tag{2.18}$$

The electric field can now be computed using a fast-Fourier-transform algorithm.

2.3 D-COIL FIELD

Two D-coils are used to represent the bends of the racetrack coil, Fig. 2.1. Using essentially the same formulation that was used for the linear coil, ψ' for the D-coil is written as in (2.6). It is convenient to express the Green's function in cylindrical polar coordinates, as

$$G(\mathbf{r},\mathbf{r}') = \frac{1}{2\pi}\sum_{m=0}^{\infty}\epsilon_m\cos[m(\phi-\phi')]\int_0^{\infty}J_m(\kappa\rho)J_m(\kappa\rho')\,\widetilde{g}\,(\kappa,z,z')\kappa\,d\kappa, \quad z<0, \tag{2.19}$$

which can be derived using an approach given by Morse and Feshbach (1). In (2.19), ϵ_m is the Neumann factor: $\epsilon_0 = 1$ and $\epsilon_m = 2$ $(m = 1,2,3,\ldots)$. For the interior of a half-space

conductor, $\widetilde{g}$ is given by (2.15). For for a slab, $\widetilde{g}$ is given by (2.16). In order to evaluate (2.6), the explicit form of $M(\mathbf{r})$ appropriate for the D-coil must be found. This form is developed as follows.

The azimuthal counter-clockwise current in a D-coil is written as

$$J_\phi(\mathbf{r}) = \begin{cases} nI, & h-c \le z \le h+c, \quad 0 \le \phi \le \pi, \quad b \le \rho \le a \\ 0, & \text{otherwise.} \end{cases} \tag{2.20}$$

where I is the current, n the number of turns per unit area. It can be deduced from (2.20), by writing

$$M(\rho,\phi,z) = \begin{cases} \mu_0 nI f_D(\rho), & h-c \le z \le h+c, \quad 0 \le \phi \le \pi, \\ 0, & \text{otherwise} \end{cases} \tag{2.21}$$

that

$$f_D(\rho) = \begin{cases} a-b, & 0 \le \rho \le b, \\ a-\rho, & b \le \rho \le a, \\ 0, & \text{otherwise} \end{cases} \tag{2.22}$$

It is now possible to obtain ψ' by substituting equations (2.19) and (2.21) into (2.6). Integration with respect to ρ', ϕ' and z' gives a summation of integrals with respect to κ:

$$\begin{aligned} \psi'(\mathbf{r}) &= nI\Big[\frac{1}{\pi}\sum_{\lambda=0}^{\infty}\frac{4}{2\lambda+1}\sin[(2\lambda+1)\phi] \\ &\quad \times \int_0^\infty [J_{2\lambda+1}(\kappa\rho)\mathcal{F}_{2\lambda+1}(a,b,\kappa)\,\widetilde{g}\,(\kappa,z,h)\sinh(\kappa c)]\,d\kappa \\ &\quad + \int_0^\infty [J_0(\kappa\rho)\mathcal{F}_0(a,b,\kappa)\,\widetilde{g}\,(\kappa,z,h)\sinh(\kappa c)]\,d\kappa\Big] \end{aligned} \tag{2.23}$$

where

$$\begin{aligned} \mathcal{F}_\nu(a,b,\kappa) &= \int_0^a f_D(\rho)J_\nu(\kappa\rho)\rho d\rho \\ &= \frac{1}{\kappa^2}\Big[a\mathcal{J}_\nu^{(1)}(\kappa a) - b\mathcal{J}_\nu^{(1)}(\kappa b)\Big] - \frac{1}{\kappa^3}\Big[\mathcal{J}_\nu^{(2)}(\kappa a) - \mathcal{J}_\nu^{(2)}(\kappa b)\Big] \end{aligned} \tag{2.24}$$

with f_D given by (2.22) and

$$\mathcal{J}_\nu^n(z) = \int_0^z x^n J_\nu(x)\,dx. \tag{2.25}$$

These functions are evaluated for $\nu > 3$ with the aid of a recursion relationship

$$(\nu-n)\mathcal{J}_{\nu+1}^n(z) = -2\nu z^n J_\nu(z) + (\nu+n)\mathcal{J}_{\nu-1}^n(z) \tag{2.26}$$

derived using Eq 11.3.6 of reference (2).

The integrals with respect to κ must be computed numerically and the summation in (2.23) truncated at a suitable order depending on the required accuracy of the result. For the double-D filament loop (3) a truncated series of five terms is sufficiently accurate in most cases and the same is true for the series in (2.23) representing the potential due to a racetrack coil bend.

From equation (2.2), the electric field in cylindrical coordinates is

$$\mathbf{E}(\mathbf{r}) = -\jmath\omega\mu_0 \left(\hat{\rho}\frac{1}{\rho}\frac{\partial}{\partial\phi} - \hat{\phi}\frac{\partial}{\partial\rho}\right)\psi'(\mathbf{r}). \tag{2.27}$$

The components of the electric field are therefore,

$$\begin{aligned} E_\rho(\mathbf{r}) &= -\frac{4\jmath\omega\mu_0 nI}{\pi\rho}\sum_{\lambda=0}^{\infty}\cos[(2\lambda+1)\phi] \\ &\quad \times \int_0^\infty J_{2\lambda+1}(\kappa\rho)\mathcal{F}_{2\lambda+1}(a,b,\kappa)\,\widetilde{g}\,(\kappa,z,z_0,h)\sinh(\kappa c)\,d\kappa \end{aligned} \tag{2.28}$$

and

$$\begin{aligned} E_\phi(\mathbf{r}) &= \jmath\omega\mu_0 nI\Bigg\{\frac{1}{\pi}\sum_{\lambda=0}^{\infty}\frac{4}{2\lambda+1}\sin[(2\lambda+1)\phi] \\ &\quad \int_0^\infty \left[\kappa J_{2\lambda}(\kappa\rho) - \frac{2\lambda+1}{\rho}J_{2\lambda+1}(\kappa\rho)\right]\mathcal{F}_{2\lambda+1}(a,b,\kappa)\,\widetilde{g}\,(\kappa,z,h)\,\sinh(\kappa c)\,d\kappa \\ &\quad -\int_0^\infty \kappa J_1(\kappa\rho)\mathcal{F}_0(a,b,\kappa)\,\widetilde{g}\,(\kappa,z,h)\sinh(\kappa c)\,d\kappa\Bigg\} \end{aligned} \tag{2.29}$$

respectively.

2.4 RESULTS

The sensor signals due to a square recess in the bottom surface of a plate of thickness 4.85 mm, Fig. 2.2, with the racetrack coil above the plate providing the excitation field has been calculated using a volume element code (4). The dimensions of the recess are 25.4 mm × 25.4 mm × 3 mm. These and other parameters are given in Table 2.1.

The sensors measure the magnetic field component normal to the surface of the conductor. Fig. 2.3, compares the variation with probe position of the normal magnetic field at a central sensor. Field values are normalized to a coil current of 1 Amp. The field variation is due to the back surface recess is plotted for different racetrack excitation coils. One has 64 mm

total straight sections, one has 24 mm total straight sections, one has 4 mm total straight sections and the other has no straight sections and is thus a circular coil. Results from the zero straight section coil using computer code for the racetrack analysis agree with results for a dedicated circular coil calculation (5). The absolute value of the z-component of the field found by simulating the response of a 33 element sensor array is shown in Fig. 2.4.

2.5 CONCLUSION

The theory for a racetrack coil in the presence of a stratified conductor has been given in two parts based on a formulation using a magnetic dipole representation of the effect of the coil. In the first part the field due to the straight sections of the track are found using a two dimensional Fourier transform, and in the second part, the field due to the semicircular bends of the track are determined using integrals containing Bessel functions. The racetrack coil geometry will be incorporated into a probe design in which an array of magnetic sensors are located along the center line of the track parallel to the straight sections. In this way the local applied field experienced by each sensor is similar yet the probe itself is compact and easy to manipulate.

ACKNOWLEDGEMENTS

This work is supported by the AFRL Materials and Manufacturing Directorate at Wright-Patterson Air Force Base under contract F33615-97-D-5271-0031 sponsored by Dr. Thomas J. Moran.

REFERENCES

[1] P. Morse and H. Feshbach, Methods of Theoretical Physics. (McGraw-Hill, New York, 1953) p. 1263.

[2] M. Abramowitz and I. A. Stegun, *Handbook of Mathematical Functions with Formulas, Graphs and Mathematical Tables* (9th printing, Dover, New York, 1970).

[3] D. McA. McKirdy, S. Cochran, G. B. Donaldson and A. McNab, Theoretical Consideration of Fatigue Crack Detection and Characterisation Using SQUID Sensors. In: R Collins W D Dover J R Bowler and K Miya (eds.), Nondestructive Testing of Materials. IOS Press, Amsterdam, p. 185 (1995).

[4] J. R. Bowler, S. A. Jenkins, H. A. Sabbagh and L. D. Sabbagh, J. Appl. Phys. 70, No. 3, p. 1107, 1991.

[5] C.V Dodd and W. E. Deeds, J. Appl. Phys., 39, 2829, 1968.

Table 2.1 Test parameters for magnetic sensor measurements on a hidden surface material-loss specimen.

Coil	
Outer radius	10.625 mm
Inner radius	1.6875 mm
Axial length	4.98 mm
Nominal lift-off	2.5825 mm
Number of turns	337 ± 1
Number of sensors	33
Height of sensors	0.869 mm
Distance between sensors	2.0 mm
Frequency	2000 Hz
Plate	
Conductivity	1.82×10^7 S/m
Thickness	4.85 mm
Flaw	
Length	25.4 mm
Width	25.4 mm
Depth	3.00 mm

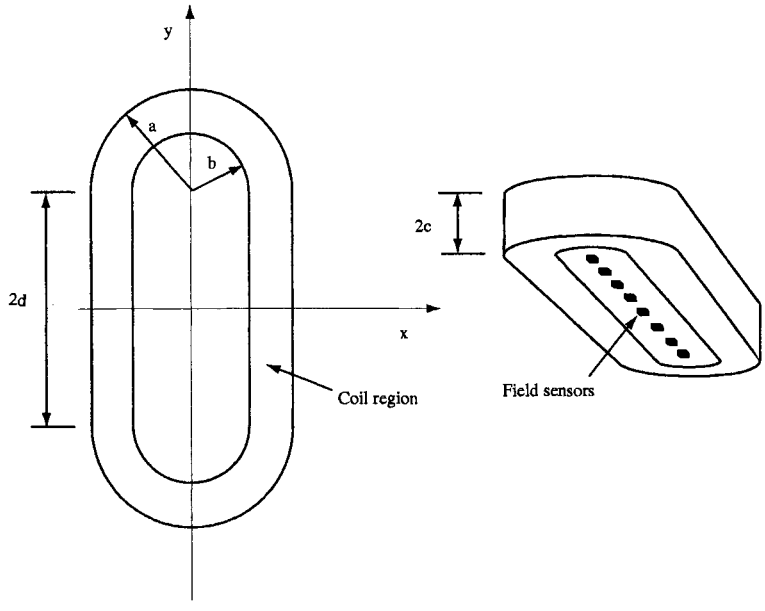

Figure 2.1 Racetrack probe showing coil geometry and magnetic field sensor array.

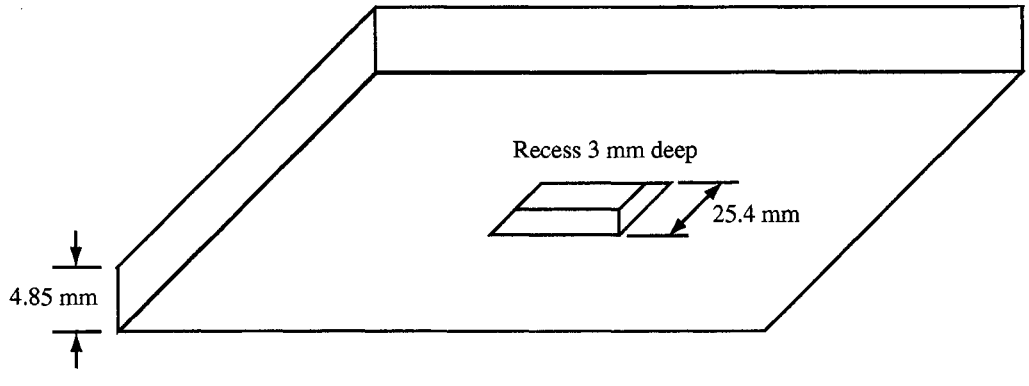

Figure 2.2 Conducting plate with a square recess.

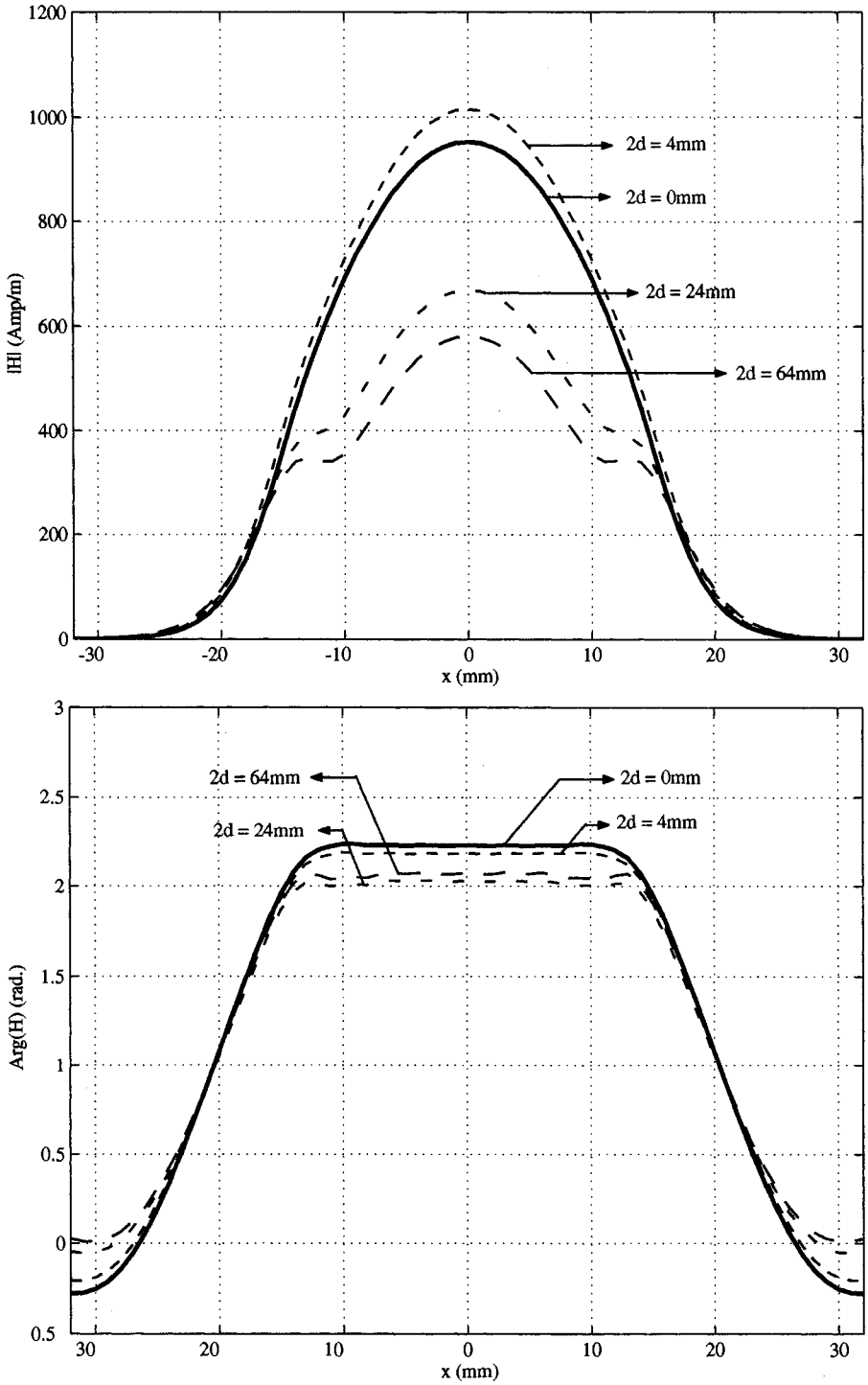

Figure 2.3 Variation with probe position of the magnitude and phase of the magnetic field at the site of a central sensor 0.89 mm from the surface of the material.

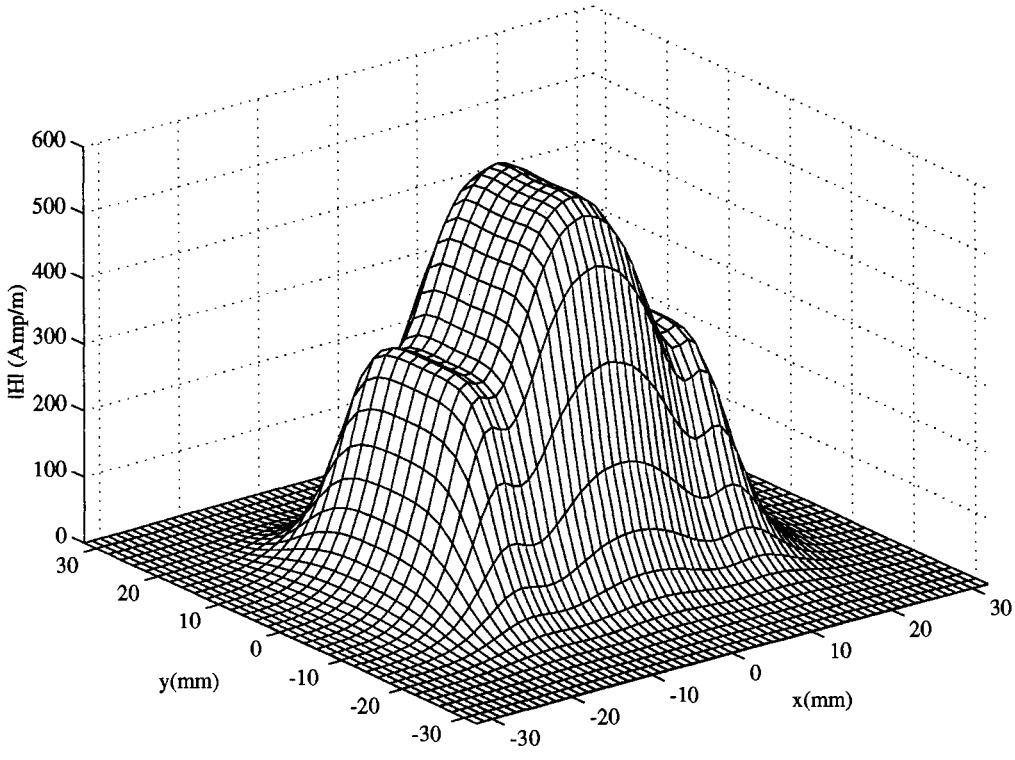

Figure 2.4 Magnitude of the magnetic field at 32 sensor sites due to race-track coil excitation of a metal plate containing a back surface recess, Fig. 2. The excitation frequency is 2000 Hz, $2d = 64$ mm (see Fig. 1) and the other probe dimensions are as given in Table 2.1.

CHAPTER 3. FLAW DISCRETIZATION USING EDGE ELEMENTS

3.1 INTRODUCTION

An eddy current problem can be solved using many different methods such as the finite element method, the finite difference time domain and the integral equation method. In the preceding chapter, an electric field based integral equation method was employed for finding the magnetic field sensor response (9). In the electric field integral equation formulation adapted here, the solution is the unknown dipole density inside the flaw or crack region due the excitation coil. Following the method of moments approach, the unknown dipole density distribution is expanded in terms of basis functions and testing functions are used for forming a matrix equation. The advantage of integral equation based techniques over other techniques is that we only need to solve for the field in the flaw region only provided the Green's function for the unflawed structure is known. In other techniques we need to discretize whole of the conductor body in order to find a solution. Because we have a small solution region, fewer unknowns are needed and a solution can be found faster than with other methods. In the integral equation based technique, the flaw is divided into cells and method of moment along with Galerkin method is used for solving for the unknowns. Typically, a piecewise constant basis function is used. As described in the previous chapter on the sensor response, rooftop shaped volume element functions are used for the discretization along with a point matching scheme for defining a matrix approximation of the integral equation. The disadvantage of this scheme is that it does not necessarily guarantee zero divergence of the electric field, which is required for the correct dipole density inside the flaw region.

An improved discretization scheme, based on edge element functions, has been developed in which the basis functions have zero divergence, (2) - (3), (24), (30). Edge element shape

functions has the property of tangential continuity across the edges and also across the surface. Hence, if we express our unknown dipole density as a linear combination of the curl of these edge element shape function then we can guarantee zero divergence and normal continuity across the facets and by doing that we should have a better convergence to the solution as compared to the previous one. A significant advantage of using edge element basis functions is that their shape can be modified to conform to the boundary of an object. This allows accurate modelling of complex geometries.

In the next few sections a detailed analysis of the basic formulation of the theory using edge based shaped function for the eddy current problem is presented. The basic formulation was developed by G. Rubinacci and A. Tamburrino, reference (30). Its numerical application for a flaw in a half-space conductor is developed in this thesis using the definitions of edge shaped basis function as given in (24).

3.2 MATRIX EVALUATION - THEORY

3.2.1 Mathematical Model

Let us assume that we have a volumetric flaw having a constant conductivity of σ_f within a three dimensional domain Ω_f in a conducting half space or a slab. Assume also that the host material is made up of a linear, isotropic, non-dispersive, non-magnetic and homogeneous material of conductivity of σ_0. With these assumptions, we can write the governing Maxwell's equations for the region inside the conducting slab for a sinusoidal time varying field, as

$$\begin{aligned} \nabla \times \mathbf{E} &= \jmath\omega\mu_0\mathbf{H} \\ \nabla \times \mathbf{H} &= \sigma(\mathbf{r})\mathbf{E} - \jmath\omega\epsilon_0\mathbf{E} \\ \nabla \cdot \mathbf{E} &= \frac{\rho}{\epsilon_0} \\ \nabla \cdot \mathbf{H} &= 0 \end{aligned} \tag{3.1}$$

and

$$\sigma(\mathbf{r}) = \begin{cases} \sigma_0, & \text{for} \quad \Omega_0 \setminus \Omega_f \\ \sigma_f, & \text{for} \quad \Omega_f \\ 0, & \text{otherwise,} \end{cases} \tag{3.2}$$

where Ω_0 is the domain of the conductor.

For an eddy current problem, we can simplify (3.1) by neglecting the displacement term, $\jmath\omega\epsilon_0\mathbf{E}$. We can rewrite Ampere's law as

$$\nabla \times \mathbf{H} = \mathbf{P} + \sigma_0\mathbf{E}, \tag{3.3}$$

where $\mathbf{P}$ is the dipole density given by

$$\mathbf{P} = (\sigma(\mathbf{r}) - \sigma_0)\mathbf{E}. \tag{3.4}$$

The dipole density will have a non-zero value only in the region of the flaw. The dipole density can be found from the integral equation (9),

$$\mathbf{P}(\mathbf{r}) = \mathbf{P}^i(\mathbf{r}) + (\sigma_0 - \sigma_f)\jmath\omega\mu_0 \int_{\Omega_f} \mathcal{G}^{ee}(\mathbf{r}|\mathbf{r}') \cdot \mathbf{P}(\mathbf{r}')d\mathbf{r}' \qquad \forall\, \mathbf{r} \in \Omega_f \tag{3.5}$$

where $\mathbf{P}^i(\mathbf{r}) = (\sigma_0 - \sigma_f)\mathbf{E}^i(\mathbf{r})$, $\mathbf{E}^i(\mathbf{r})$ is the incident electric field inside the conductor and $\mathcal{G}^{ee}(\mathbf{r}|\mathbf{r}')$ is the electric-electric dyadic Green's function which transforms an electric source into the electric field.

By assuming that there is no impressed charge density inside the flaw region, we will have

$$\nabla \cdot \mathbf{E} = 0, \qquad \forall\ \overset{\circ}{\Omega}_f \tag{3.6}$$

where $\overset{\circ}{\Omega}_f$ represents the volume inside the flaw region excluding the boundary where charge resides. From (3.4) and (3.6) we have,

$$\nabla \cdot \mathbf{P} = 0, \qquad \forall\ \overset{\circ}{\Omega}_f \tag{3.7}$$

which means that the $\mathbf{P}$ is solenoidal in $\overset{\circ}{\Omega}_f$.

3.2.2 Numerical Model

Galerkin's method is applied to (3.5) for finding numerically the dipole density $\mathbf{P}$ in the flaw region. The solenoidal property of $\mathbf{P}$ in $\overset{\circ}{\Omega}_f$ can be ensured by expressing it in terms of electric vector potential $\mathbf{U}$ as,

$$\mathbf{P} = \gamma(\mathbf{r}) \nabla \times \mathbf{U} \tag{3.8}$$

where,

$$\gamma(\mathbf{r}) = \begin{cases} 1, & \forall\, \mathbf{r} \in \overset{\circ}{\Omega}_f \\ 0, & \text{otherwise} \end{cases} \tag{3.9}$$

Permissible vector potentials differ by an irrotational vector field. To ensure that the vector potential is uniquely defined one needs only to eliminate *all* irrotational fields from its functional space. In this way, the gauge condition, to be applied later, will make the solution field $\mathbf{U}$ unique. The electric vector potential, $\mathbf{U}$, can be approximated by an expansion in terms of 1-Whitney edge elements (2), (6). Thus, we can write[1]

$$\mathbf{U} = \sum_{e=1}^{E} U_e \mathbf{N}_e, \tag{3.10}$$

where $\mathbf{N}_e$'s are the edge element based shape functions, e represents and edge of the discretization mesh and E are the number of mesh edges. Combining (3.8) and (3.10) gives[2]

$$\mathbf{P} = \nabla \times \mathbf{U} = \sum_{e=1}^{E} U_e \nabla \times \mathbf{N}_e \tag{3.11}$$

Further discussion on edge element basis function is given in the next appendix. Galerkin's method applied to (3.5) gives,

$$(\mathbf{R} - \jmath\omega\mathbf{L})\mathbf{U} = \mathbf{V}^0 \tag{3.12}$$

where,

$$(\mathbf{V}^0)_i = \int_{\Omega_f} \nabla \times \mathbf{N}_i(\mathbf{r}) \cdot \mathbf{E}^{(0)}(\mathbf{r}) d\mathbf{r} \tag{3.13}$$

$$(\mathbf{R})_{ij} = \frac{1}{\sigma_0 - \sigma_f} \int_{\Omega_f} \nabla \times \mathbf{N}_i(\mathbf{r}) \cdot \nabla \times \mathbf{N}_j(\mathbf{r}) d\mathbf{r} \tag{3.14}$$

[1] The edge elements have a zero divergence and a nonzero curl. Hence, the expansion of $\mathbf{U}$ using edge elements guarantees the tangential continuity of $\mathbf{U}$ across the edges but also guarantees the tangential continuity across the surface.

[2] the form of the expansion guarantee that $\mathbf{P}$ will have a zero divergence. Hence the normal continuity across facets is also guaranteed.

$$(\mathbf{L})_{ij} = \mu_0 \int_{\Omega_f} \int_{\Omega_f} \nabla \times \mathbf{N}_i(\mathbf{r}) \cdot \mathcal{G}^{ee}(\mathbf{r}|\mathbf{r}') \cdot \nabla \times \mathbf{N}_j(\mathbf{r}') d\mathbf{r}' d\mathbf{r} \tag{3.15}$$

The dyadic Green's function $\mathcal{G}^{ee}$ can be written as (9),

$$\mathcal{G}^{ee}(\mathbf{r}|\mathbf{r}') = \mathcal{G}_0^{ee}(\mathbf{r}|\mathbf{r}') + \delta\mathcal{G}^{ee}(\mathbf{r}|\mathbf{r}') \tag{3.16}$$

where $\mathcal{G}_0^{ee}$ is the free space electric-electric dyadic Green's function with conductivity of σ_0, (33), and $\delta\mathcal{G}^{ee}$ is a continuous function in $\Omega_0 \backslash \Omega_f$, (9). The free space dyadic Green's function can be written as,

$$\mathcal{G}_0^{ee}(\mathbf{r}|\mathbf{r}') = [\mathcal{I} + \frac{1}{k^2}\nabla\nabla] G_0(\mathbf{r}|\mathbf{r}') \tag{3.17}$$

where $\mathcal{I}$ is the unity dyad and

$$G_0(\mathbf{r}|\mathbf{r}') = \frac{e^{-\jmath k|\mathbf{r}-\mathbf{r}'|}}{4\pi|\mathbf{r}-\mathbf{r}'|}, \qquad k^2 = -\jmath\omega\mu_0\sigma_0 \tag{3.18}$$

The term $\delta\mathcal{G}^{ee}(\mathbf{r}|\mathbf{r}')$ for a half space conductor can be express as the sum of an image term and a transverse electric term, $\frac{1}{k^2}[\nabla \times \hat{z}[\nabla' \times \hat{z}V(\mathbf{r}|\mathbf{r}')]]$ accounting for the partial reflection from the interface, (9). Thus

$$\delta\mathcal{G}^{ee}(\mathbf{r}|\mathbf{r}') = [\mathcal{I} + \frac{1}{k^2}\nabla\nabla] \cdot \mathcal{I}' G_0(\mathbf{r}|\mathbf{r}' - 2\hat{z}z') + \frac{1}{k^2}[\nabla \times \hat{z}[\nabla' \times \hat{z}V(\mathbf{r}|\mathbf{r}')]] \tag{3.19}$$

where $\mathcal{I}' = \hat{x}\hat{x} + \hat{y}\hat{y} - \hat{z}\hat{z}$ and

$$V(\mathbf{r}|\mathbf{r}') = \pm\frac{1}{2\pi} L_z(k, \rho, |z+z'|) - 2G_0(\mathbf{r}|\mathbf{r}' - 2\hat{z}z') \tag{3.20}$$

where $\rho^2 = (x-x')^2 + (y-y')^2$. The $+$ sign holds if $z + z' < 0$ and $-$ sign if $z + z > 0$. L_z represents the partial derivative of L which is defined by Foster-Lien integral.

We can rewrite (3.15) as,

$$\mathbf{L} = \mathbf{L}_0 + \delta\mathbf{L} \tag{3.21}$$

where

$$(\mathbf{L}_0)_{ij} = \mu_0 \int_{\Omega_f} \int_{\Omega_f} \nabla \times \mathbf{N}_i(\mathbf{r}) \cdot \mathcal{G}_0^{ee}(\mathbf{r}|\mathbf{r}') \cdot \nabla \times \mathbf{N}_j(\mathbf{r}') d\mathbf{r}' d\mathbf{r} \tag{3.22}$$

and

$$(\delta\mathbf{L})_{ij} = \mu_0 \int_{\Omega_f} \int_{\Omega_f} \nabla \times \mathbf{N}_i(\mathbf{r}) \cdot \delta\mathcal{G}^{ee}(\mathbf{r}|\mathbf{r}') \cdot \nabla \times \mathbf{N}_j(\mathbf{r}') d\mathbf{r}' d\mathbf{r} \tag{3.23}$$

As $\delta\mathbf{L}$ doesn't contain any singularities, standard numerical methods can be used for its computation. Whereas, for the case of $\mathbf{L}_0$, which contains a singularity, it is helpful do divide the integration into volume term and surface term,

$$\mathbf{L}_0 = \mathbf{L}_0^V + \mathbf{L}_0^S \tag{3.24}$$

where

$$(\mathbf{L}_0^V)_{ij} = \mu_0 \int_{\Omega_f} \int_{\Omega_f} \nabla \times \mathbf{N}_i(\mathbf{r}) \cdot G_0(\mathbf{r}|\mathbf{r}') \nabla \times \mathbf{N}_j(\mathbf{r}') d\mathbf{r}' d\mathbf{r} \tag{3.25}$$

and the surface term is derived from

$$(\mathbf{L}_0^S)_{ij} = \frac{\mu_0}{k^2} \int_{\Omega_f} \int_{\Omega_f} \nabla \times \mathbf{N}_i(\mathbf{r}) \cdot \nabla\nabla G_0(\mathbf{r}|\mathbf{r}') \cdot \nabla \times \mathbf{N}_j(\mathbf{r}') d\mathbf{r}' d\mathbf{r} \tag{3.26}$$

For the surface term, the hyper-singular term $\nabla\nabla G_0(\mathbf{r}|\mathbf{r}')$ acts on a vector field in the following way,

$$\nabla\nabla G_0(\mathbf{r}|\mathbf{r}') \cdot \mathbf{w}(\mathbf{r}) = \nabla \left[\nabla \cdot \left\{ \int G_0(\mathbf{r}|\mathbf{r}')\, \mathbf{w}(\mathbf{r}) d\mathbf{r} \right\} \right] \tag{3.27}$$

Hence we can write (3.26) as,

$$(\mathbf{L}_0^S)_{ij} = \frac{\mu_0}{k^2} \int_{\Omega_f} \mathbf{P}_i(\mathbf{r}) \cdot \nabla \left[\nabla \cdot \left\{ \int_{\Omega_f} G_0(\mathbf{r}|\mathbf{r}') \mathbf{P}_j(\mathbf{r}') d\mathbf{r}' \right\} \right] d\mathbf{r} \tag{3.28}$$

Because

$$\nabla \cdot [\mathbf{A}\, \psi] = \mathbf{A} \cdot \nabla\psi \qquad \text{if} \quad \nabla \cdot \mathbf{A} = 0 \tag{3.29}$$

therefore, (3.28) reduces to,

$$(\mathbf{L}_0^S)_{ij} = \frac{\mu_0}{k^2} \int_{\Omega_f} \nabla \cdot \left[\mathbf{P}_i(\mathbf{r}) \nabla \cdot \left\{ \int_{\Omega_f} G_0(\mathbf{r}|\mathbf{r}') \mathbf{P}_j(\mathbf{r}') d\mathbf{r}' \right\} \right] d\mathbf{r} \tag{3.30}$$

By using divergence theorem on both the integrals and noting that $\nabla \cdot [G_0(\mathbf{r}|\mathbf{r}')\mathbf{P}_j(\mathbf{r}')] = -\nabla' \cdot [G_0(\mathbf{r}|\mathbf{r}')\mathbf{P}_j(\mathbf{r}')]$, (3.30) reduces further to,

$$(\mathbf{L}_0^S)_{ij} = -\frac{\mu_0}{k^2} \oint_{S_i} \oint_{S_j} [\hat{\mathbf{n}}(\mathbf{r}) \cdot \mathbf{P}_i(\mathbf{r})]\, G_0(\mathbf{r}|\mathbf{r}')\, [\hat{\mathbf{n}}(\mathbf{r}') \cdot \mathbf{P}_j(\mathbf{r}')] d\mathbf{S}' d\mathbf{S} \tag{3.31}$$

where S_i and S_j are the surfaces of the flaw element for Ω_i and Ω_j respectively and $\hat{\mathbf{n}}(\mathbf{r})$ represents an outward normal direction of a surface.

3.2.2.1 Volume Matrix Evaluation - $\mathbf{L}_0^V$

For simplicity, first consider a one dimensional problem in which the moment method is applied with the basis functions $\psi_l(x)$, which are non-zero over the range $x_l < x < x_l + \Delta x$, where Δx is the size of the unit cell, $x_l = l\Delta x$ and $l = 0, 1, 2, \ldots N-1$. Suppose also that the basis functions have the property $\psi_{k-1}(x) = \psi_k(x - \Delta x)$. By applying the moment method, matrix elements are defined by,

$$I_{kK} = \int_{x_k}^{x_k+\Delta x} \int_{x_K}^{x_K+\Delta x} \phi_k(x) G(x - x') \psi_K(x') dx' dx \tag{3.32}$$

where ϕ_k represents testing function which are non-zero over the range $x_k < x < x_k + \Delta x$, where $k = 0, 1, 2, \ldots N-1$. We can rewrite (3.32) by expanding the integrals from $-\infty$ to ∞ as the basis function is zero outside its specified range. Hence

$$I_{kK} = \int_{-\infty}^{\infty} \int_{-\infty}^{\infty} \phi_k(x) G(x - x') \psi_K(x') dx' dx \tag{3.33}$$

Let $x_0 = x - x'$ and write $\phi_l(x) = \phi_0(x - x_l)$, to give,

$$I_{kK} = \int_{-\infty}^{\infty} \int_{-\infty}^{\infty} \phi_0(x - x_k) G(x_0) \psi_K(x - x_0) dx_0 dx \tag{3.34}$$

Now let $x - x_k = x'$, hence

$$I_{kK} = \int_{-\infty}^{\infty} \int_{-\infty}^{\infty} \phi_0(x') G(x_0) \psi_K(x' - x_0 + x_k) dx_0 dx'. \tag{3.35}$$

By assuming $x_k - x_0 = x_0'$, we can rewrite (3.34) as,

$$I_{kK} = \int_{-\infty}^{\infty} \int_{-\infty}^{\infty} \phi_0(x') G(x_k - x_0') \psi_K(x' + x_0') dx_0' dx'. \tag{3.36}$$

Define,

$$\beta_K(x_0') = \int_{-\infty}^{\infty} \phi_0(x) \psi_K(x' + x_0') dx'. \tag{3.37}$$

Hence, (3.36) reduces to

$$I_{kK} = \int_{-\infty}^{\infty} \beta_K(x_0') G(x_k - x_0') dx_0', \tag{3.38}$$

Hence I_{kK}, defined in (3.32), can be computed from (3.38), which is equivalent to having β_j as the basis functions and testing with delta functions. Thus (3.38) is effectively a point matching formulae for a solution expanded in terms of β_j.

For the corresponding three dimensional case, the matrix elements with a convolution kernel are defined as,

$$L_{klm,KLM} = \int_{V_{klm}} \int_{V_{KLM}} \phi_{klm}(\mathbf{r}) G(\mathbf{r} - \mathbf{r}') \psi_{KLM}(\mathbf{r}') d\mathbf{r}' d\mathbf{r} \tag{3.39}$$

where V_{klm} is the volume defining the support of $\phi_{klm}(\mathbf{r})$ and V_{KLM} is the volume defining the support of $\phi_{klm}(\mathbf{r})$. By generalizing the above argument from the one dimensional moment method case, it is found that

$$L_{klm,KLM} = \int_{\Omega_{KLM}} G_0(\mathbf{r_{klm}}|\mathbf{r}') \beta_{KLM}(\mathbf{r}') d\mathbf{r}' \tag{3.40}$$

where Ω_{KLM} is the volume defined by $(K-1)\Delta x \leq x < (K+1)\Delta x$, $(L-1)\Delta y \leq y < (K+1)\Delta y$, $(K-1)\Delta x \leq x < (K+1)\Delta x$. With the origin of the coordinate system suitably chosen we can write (3.40) as,

$$L_{klm,KLM} = \int_{\Omega_{klm}} G(\mathbf{0}|\mathbf{r}') \beta_{klm}(\mathbf{r}') d\mathbf{r}' \tag{3.41}$$

Hence,

$$(\mathbf{L}_0^V)_{ij} = \mu_0 \sum_{\epsilon} \sum_{\epsilon'} \int_{\Omega_{klm}} G_0(\mathbf{0}|\mathbf{r}') \beta_{\epsilon\epsilon',klm}(\mathbf{r}') d\mathbf{r}' \tag{3.42}$$

where ϵ and ϵ' $(\epsilon, \epsilon' = 1, 2, \ldots 12)$ are the local edge indices for the ith and jth global mesh edges and $\beta_{\epsilon\epsilon',klm}(\mathbf{r}')$ is the product of $\beta_k(x')$, $\beta_l(y')$ and $\beta_m(z')$, (3.37).

3.3 EDGE ELEMENT EXPANSION

3.3.1 Theory

The edge element vectors, $\mathbf{N}_e$, are defined as the union of $\mathbf{N}^{(x)}_{\epsilon,\,klm}$, $\mathbf{N}^{(y)}_{\epsilon,\,klm}$, and $\mathbf{N}^{(z)}_{\epsilon,\,klm}$, where i is the local edge number, 1 to 12, of a parallelepiped at the node (k, l, m). For a simple geometry of parallelepiped at the node (k, l, m), the edge element vectors are given by (24), in normalized coordinates, Fig. 3.1, as

$$\mathbf{N}^{(x)}_{1,\,klm}(x, y, z) = \hat{x} P_k(x)(P_l(y) - \chi_l(y))(P_m(z) - \chi_m(z)) \tag{3.43}$$

$$\mathbf{N}^{(x)}_{2,\,klm}(x, y, z) = \hat{x} P_k(x)\chi_l(y)(P_m(z) - \chi_m(z)) \tag{3.44}$$

$$\mathbf{N}^{(x)}_{3,\,klm}(x, y, z) = \hat{x} P_k(x)(P_l(y) - \chi_l(y))\chi_m(z) \tag{3.45}$$

$$\mathbf{N}^{(x)}_{4,\,klm}(x,y,z) = \hat{x}P_k(x)\chi_l(y)\chi_m(z) \tag{3.46}$$

$$\mathbf{N}^{(y)}_{5,\,klm}(x,y,z) = \hat{y}P_l(y)(P_m(z)-\chi_m(z))(P_k(x)-\chi_k(x)) \tag{3.47}$$

$$\mathbf{N}^{(y)}_{6,\,klm}(x,y,z) = \hat{y}P_l(y)\chi_m(z)(P_k(x)-\chi_k(x)) \tag{3.48}$$

$$\mathbf{N}^{(y)}_{7,\,klm}(x,y,z) = \hat{y}P_l(y)(P_m(z)-\chi_m(z))\chi_k(x) \tag{3.49}$$

$$\mathbf{N}^{(y)}_{8,\,klm}(x,y,z) = \hat{y}P_l(y)\chi_m(z)\chi_k(x) \tag{3.50}$$

$$\mathbf{N}^{(z)}_{9,\,klm}(x,y,z) = \hat{z}P_m(z)(P_k(x)-\chi_k(x))(P_l(y)-\chi_l(y)) \tag{3.51}$$

$$\mathbf{N}^{(z)}_{10,\,klm}(x,y,z) = \hat{z}P_m(z)\chi_k(x)(P_l(y)-\chi_l(y)) \tag{3.52}$$

$$\mathbf{N}^{(z)}_{11,\,klm}(x,y,z) = \hat{z}P_m(z)(P_k(x)-\chi_k(x))\chi_l(y) \tag{3.53}$$

$$\mathbf{N}^{(z)}_{12,\,klm}(x,y,z) = \hat{z}P_m(z)\chi_k(x)\chi_l(y) \tag{3.54}$$

where, $k = 0,1,2\ldots N_x-1$, $l = 0,1,2\ldots N_y-1$ and $m = 0,1,2\ldots N_z-1$, and,

$$P_j(q) = \begin{cases} 1, & \text{for} \quad 0 \le (q-j) < 1 \\ 0, & \text{otherwise.} \end{cases}$$

$$= P_0(q-j) \tag{3.55}$$

$$\chi_j(q) = \begin{cases} q-j, & \text{for} \quad 0 \le (q-j) < 1 \\ 0, & \text{otherwise} \end{cases}$$

$$= \chi_0(q-j) \tag{3.56}$$

Outside the specified range, the edge vectors are zero. To change from normalized coordinate to non-normalized coordinate, one simply replaces x, y and z with x/l_x, y/l_y and z/l_z where l_x, l_y and l_z are the dimensions of the unit cell. In normalized form, the nodal coordinates are (k,l,m).

To ensure a unique solution of dipole density, $\mathbf{P}$, which is solenoidal in nature (3.8), we need to impose a gauge condition to remove all irrotational field components from its functional space. In edge element theory, the nodal shape function N_k, which is associated with the kth node of a parallelepiped, is defined as continuous, piecewise trilinear function (2). The gradient

of the nodal shape function can be expressed as a linear combination of edge shape functions. Hence, in general for a kth node we can write,

$$\nabla N_k = \sum_{e=1}^{E} G_{ek} \mathbf{N}_e \tag{3.57}$$

where E is the number of edges. Similarly, a set of shape functions $\mathbf{S}_f$ associated with the faces of the elements can introduced, (2). For each oriented face $f = \{i, j, k\} = \{j, k, i\} = \{k, i, j\}$ having three vertices, the nodes i, j, k, we have

$$\mathbf{S}_f = 2(N_i \nabla N_j \times \nabla N_k + N_j \nabla N_k \times \nabla N_i + N_k \nabla N_i \times \nabla N_j) \tag{3.58}$$

Therefore for an edge e, we can define,

$$\nabla \times \mathbf{N}_e = \sum_{f=1}^{F} C_{fe} \mathbf{S}_f \tag{3.59}$$

where F is the number of faces. Hence we can express (3.11) in terms of face element shape functions as,

$$\mathbf{P} = \sum_{e=1}^{E} U_e \nabla \times \mathbf{N}_e = \sum_{e=1}^{E} \sum_{f=1}^{F} C_{fe} U_e \mathbf{S}_f = \sum_{f=1}^{F} P_f \mathbf{S}_f \tag{3.60}$$

Thus, we can write

$$\underline{\underline{C}}\, \underline{U} = \underline{P} \tag{3.61}$$

where, $\underline{\underline{C}}$ is a $E \times F$ coefficient matrix, $\mathbf{U}$ is a $1 \times E$ coefficient matrix and $\underline{P}$ is a $1 \times F$ coefficient matrix and,

$$\nabla \times \nabla N_k = \sum_{f=1}^{F} (\underline{\underline{C}}\, \underline{\underline{G}})_{fk} \mathbf{S}_f = 0 \tag{3.62}$$

Hence,

$$\underline{\underline{C}}\, \underline{\underline{G}} = \underline{\underline{0}} \tag{3.63}$$

where $\underline{\underline{0}}$ is a zero matrix. Hence, from equation (3.63) it follows that by adding any linear combination of columns of $\underline{\underline{G}}$ to $\underline{U}$, the sum will be a solution of equation (3.61). Hence, for this particular case, imposing a gauge condition is equivalent to having a unique solution to equation (3.61).

From the graph theory, (16) and (19), we know that the rank [3] of the $E \times N_p$ matrix $\underline{\underline{G}}$ is $N_p - 1$, where N_p are the number of nodes in the graph, and for the $F \times E$ matrix $\underline{\underline{C}}$ the

[3]Rank means the minimum number of linearly independent equations

rank is $E - N_p + 1$. The uniqueness of equation (3.61) is guaranteed if $\mathbf{U}$ in equation (3.10) is represented by $E - N_p + 1$ degrees of freedom, i.e. $\mathbf{U}$ is represented by $E - N_p + 1$ unknowns. To make the solution of (3.61) unique, we can eliminate edges, equivalent to removing a linear equation of the graph one by one until no solution of $\underline{\underline{G}}$ can be found satisfying (3.63), hence by further adding any linear combination of columns of $\underline{\underline{G}}$ to $\underline{U}$ will result in a new solution. The number of edges to be removed is $N_p - 1$, the same number of edges as that of the number of tree edges. Therefore, we can use only the cotree edges to reduce the set of equations and ensure a unique solution of the dipole densities.

For a simple geometry of parallelepipeds, the cotree edges can consists of the edges that lie in the $\hat{x}$ and $\hat{y}$ directions, Fig. 3.2. Therefore, the curl of the $\mathbf{N}_e$ that are in the cotree is given by,

$$
\begin{aligned}
\nabla \times [\mathbf{N}^{(x)}_{1,\,klm}(x,y,z)] &= P_k(x)\,[\hat{y}(P_l(y) - \chi_l(y))(\chi'_m(z) - P_m(z)) - \\
&\qquad \hat{z}(P_m(z) - \chi_m(z))(\chi'_l(y) - P_l(y))] \\
\nabla \times [\mathbf{N}^{(x)}_{2,\,klm}(x,y,z)] &= P_k(x)\,[\hat{y}\chi_l(y)(\chi'_m(z) - P_m(z)) - \\
&\qquad \hat{z}(P_m(z) - \chi_m(z))(P_l(y) - \chi'_{l+1}(y))] \\
\nabla \times [\mathbf{N}^{(x)}_{3,\,klm}(x,y,z)] &= P_k(x)\,[\hat{y}(P_l(y) - \chi_l(y))(P_m(z) - \chi'_{m+1}(z)) - \\
&\qquad \hat{z}\chi_m(z)(\chi'_l(y) - P_l(y))] \\
\nabla \times [\mathbf{N}^{(x)}_{4,\,klm}(x,y,z)] &= P_k(x)\,[\hat{y}\chi_l(y)(P_m(z) - \chi'_{m+1}(z)) - \\
&\qquad \hat{z}\chi_m(z)(P_l(y) - \chi'_{l+1}(y))]
\end{aligned}
$$

$$
\begin{aligned}
\nabla \times [\mathbf{N}^{(y)}_{5,\,klm}(x,y,z)] &= P_l(y)\,[\hat{z}(P_m(z) - \chi_m(z))(\chi'_k(x) - P_k(x)) - \\
&\qquad \hat{x}(P_k(x) - \chi_k(x))(\chi'_m(z) - P_m(z))] \\
\nabla \times [\mathbf{N}^{(y)}_{6,\,klm}(x,y,z)] &= P_l(y)\,[\hat{z}\chi_m(z)(\chi'_k(x) - P_k(x)) - \\
&\qquad \hat{x}(P_k(x) - \chi_k(x))(P_m(z) - \chi'_{m+1}(z))] \\
\nabla \times [\mathbf{N}^{(y)}_{7,\,klm}(x,y,z)] &= P_l(y)\,[\hat{z}(P_m(z) - \chi_m(z))(P_k(x) - \chi'_{k+1}(x)) - \\
&\qquad \hat{x}\chi_k(x)(\chi'_m(z) - P_m(z))]
\end{aligned}
$$

$$\nabla \times [\mathbf{N}^{(y)}_{8,\,klm}(x,y,z)] = P_l(y)\,[\hat{z}\chi_m(z)(P_k(x) - \chi'_{k+1}(x)) - \hat{x}\chi_k(x)(P_m(z) - \chi'_{m+1}(z))] \tag{3.64}$$

where

$$\chi'_j(q) = \delta(q-j) = \chi'_0(q-j) \tag{3.65}$$

The domain of an edge element is four cells. In two neighboring cells the edge element shape function value changes from 0 to 1 to 0 linearly. Hence, if we consider the span of an edge shaped basis function over the two neighboring cells and redefine our edge shaped basis function such that its value goes from 0 to 1 and again 0, which is equivalent to rooftop function, then the curl of the basis function doesn't contain a delta term which is present when we have just one cell and the definition of the basis function changes from 0 to 1, 1 at the edge itself, and goes to zero just after the edge, i.e outside the cell. Therefore, for the computational purpose we can neglect the delta terms from the $\nabla \times \mathbf{N}_e$ for the cells that are not associated with surface of the flaw. The surface delta terms will be taken care by the surface integral of (3.31). Hence, the reduced set of (3.64) will be,

$$\begin{aligned}
\nabla \times [\mathbf{N}^{(x)}_{1,\,klm}(x,y,z)] &= P_k(x)\,[-\hat{y}(P_l(y) - \chi_l(y))P_m(z) + \hat{z}(P_m(z) - \chi_m(z))P_l(y)] \\
\nabla \times [\mathbf{N}^{(x)}_{2,\,klm}(x,y,z)] &= P_k(x)\,[-\hat{y}\chi_l(y)P_m(z) - \hat{z}(P_m(z) - \chi_m(z))P_l(y)] \\
\nabla \times [\mathbf{N}^{(x)}_{3,\,klm}(x,y,z)] &= P_k(x)\,[\hat{y}(P_l(y) - \chi_l(y))P_m(z) + \hat{z}\chi_m(z)P_l(y)] \\
\nabla \times [\mathbf{N}^{(x)}_{4,\,klm}(x,y,z)] &= P_k(x)\,[\hat{y}\chi_l(y)P_m(z) - \hat{z}\chi_m(z)P_l(y)]
\end{aligned}$$

$$\begin{aligned}
\nabla \times [\mathbf{N}^{(y)}_{5,\,klm}(x,y,z)] &= P_l(y)\,[-\hat{z}(P_m(z) - \chi_m(z))P_k(x) + \hat{x}(P_k(x) - \chi_k(x))P_m(z)] \\
\nabla \times [\mathbf{N}^{(y)}_{6,\,klm}(x,y,z)] &= P_l(y)\,[-\hat{z}\chi_m(z)P_k(x) - \hat{x}(P_k(x) - \chi_k(x))P_m(z)] \\
\nabla \times [\mathbf{N}^{(y)}_{7,\,klm}(x,y,z)] &= P_l(y)\,[\hat{z}(P_m(z) - \chi_m(z))P_k(x) + \hat{x}\chi_k(x)P_m(z)] \\
\nabla \times [\mathbf{N}^{(y)}_{8,\,klm}(x,y,z)] &= P_l(y)\,[\hat{z}\chi_m(z)P_k(x) - \hat{x}\chi_k(x)P_m(z)]
\end{aligned} \tag{3.66}$$

3.3.2 Computation of Matrix Terms

For the computation of the matrix terms in (3.12), the flaw is divided into volumetric cells. Only the cotree edges of the graph are labelled. Each edge has been assigned two indices, one is local to the cell and the other is global. The interaction of one local edge of a volumetric cell is taken with local edge of another volumetric cell and finally the interaction is added to the respective global edge number interaction [4].

3.3.2.1 Computation of $\mathbf{V}^0$ Matrix Terms

As the unperturbed electric field is transverse to the z-direction inside the conductor, we only need to consider the corresponding $\hat{x}$ and $\hat{y}$ components of the $\nabla \times \mathbf{N}_e$ in evaluating (3.13). For a particular edge, as the $\nabla \times \mathbf{N}_e$ is a constant or a linear function in x and y, we can express the integration as a summation of values at 6 fixed points inside the cell with each weighted by $\frac{1}{6}$ [see Eq. 25.4.67, page 895 of (1)]. For a particular cell at normalized coordinates of (k, l, m), we can take the center of each face as the fixed point for evaluating the integration, Fig. 3.1, namely points A to F. The value of $\nabla \times \mathbf{N}_e$ at these points will be $\pm\frac{1}{2}$. Hence, for local edge numbers from 1 to 8,

$$
\begin{aligned}
\int_{V_{klm}} \nabla \times \mathbf{N}^{(x)}_{1,\,klm}(\mathbf{r}) \cdot \mathbf{E}^{(0)}(\mathbf{r}) d\mathbf{r} &= \frac{-V_0}{6}[E^0_{A,y} + \frac{1}{2}(E^0_{C,y} + E^0_{D,y} + E^0_{E,y} + E^0_{F,y})] \\
\int_{V_{klm}} \nabla \times \mathbf{N}^{(x)}_{2,\,klm}(\mathbf{r}) \cdot \mathbf{E}^{(0)}(\mathbf{r}) d\mathbf{r} &= \frac{-V_0}{6}[E^0_{B,y} + \frac{1}{2}(E^0_{C,y} + E^0_{D,y} + E^0_{E,y} + E^0_{F,y})] \\
\int_{V_{klm}} \nabla \times \mathbf{N}^{(x)}_{3,\,klm}(\mathbf{r}) \cdot \mathbf{E}^{(0)}(\mathbf{r}) d\mathbf{r} &= \frac{V_0}{6}[E^0_{A,y} + \frac{1}{2}(E^0_{C,y} + E^0_{D,y} + E^0_{E,y} + E^0_{F,y})] \\
\int_{V_{klm}} \nabla \times \mathbf{N}^{(x)}_{4,\,klm}(\mathbf{r}) \cdot \mathbf{E}^{(0)}(\mathbf{r}) d\mathbf{r} &= \frac{V_0}{6}[E^0_{B,y} + \frac{1}{2}(E^0_{C,y} + E^0_{D,y} + E^0_{E,y} + E^0_{F,y})]
\end{aligned}
$$

$$
\begin{aligned}
\int_{V_{klm}} \nabla \times \mathbf{N}^{(y)}_{5,\,klm}(\mathbf{r}) \cdot \mathbf{E}^{(0)}(\mathbf{r}) d\mathbf{r} &= \frac{-V_0}{6}[E^0_{C,x} + \frac{1}{2}(E^0_{A,x} + E^0_{B,x} + E^0_{E,x} + E^0_{F,x})] \\
\int_{V_{klm}} \nabla \times \mathbf{N}^{(y)}_{6,\,klm}(\mathbf{r}) \cdot \mathbf{E}^{(0)}(\mathbf{r}) d\mathbf{r} &= \frac{V_0}{6}[E^0_{C,x} + \frac{1}{2}(E^0_{A,x} + E^0_{B,x} + E^0_{E,x} + E^0_{F,x})] \\
\int_{V_{klm}} \nabla \times \mathbf{N}^{(y)}_{7,\,klm}(\mathbf{r}) \cdot \mathbf{E}^{(0)}(\mathbf{r}) d\mathbf{r} &= \frac{-V_0}{6}[E^0_{D,x} + \frac{1}{2}(E^0_{A,x} + E^0_{B,x} + E^0_{E,x} + E^0_{F,x})]
\end{aligned}
$$

[4] For a given cell we can have 8 cotree edges, 4 in each $\hat{x}$ and $\hat{y}$ directions, and we have $E - N_p + 1$ global edges. In terms of number of discretization cells, N_x, N_y and N_z in the x, y and z directions respectively, we can rewrite $E - N_p + 1$ as $2N_xN_yN_z + N_xN_y + N_yN_z + N_zN_x$.

$$\int_{V_{klm}} \nabla \times \mathbf{N}^{(y)}_{8,\,klm}(\mathbf{r}) \cdot \mathbf{E}^{(0)}(\mathbf{r}) d\mathbf{r} \;=\; \frac{V_0}{6}[E^0_{D,x} + \frac{1}{2}(E^0_{A,x} + E^0_{B,x} + E^0_{E,x} + E^0_{F,x})] \quad (3.67)$$

where V_0 = Volume of a cell of the flaw region, $E^0_{A,x} = \hat{x} \cdot \mathbf{E}^0_A$ and similarly others. Hence,

$$(\mathbf{V}^0)_i = \sum_{\epsilon} \int_{V_{klm}} \nabla \times \mathbf{N}^{(x)}_{\epsilon,\,klm}(\mathbf{r}) \cdot \mathbf{E}^{(0)}(\mathbf{r}) d\mathbf{r} \quad (3.68)$$

where ϵ ($\epsilon = 1, 2, 3, 4$) are the local edge indices for the ith global mesh edges for x-directed edges and for y-directed edges,

$$(\mathbf{V}^0)_i = \sum_{\epsilon} \int_{V_{klm}} \nabla \times \mathbf{N}^{(y)}_{\epsilon,\,klm}(\mathbf{r}) \cdot \mathbf{E}^{(0)}(\mathbf{r}) d\mathbf{r} \quad (3.69)$$

where ϵ ($\epsilon = 5, 6, 7, 8$) are the local edge indices for the ith global mesh edges.

3.3.2.2 Computation of R Matrix Terms

In the **R** matrix, (3.14), we are requried to integrate a dot product of the form $\nabla \times \mathbf{N}_i \cdot \nabla \times \mathbf{N}_j$. These integrals will be evaluated for a particular cell and the contributions from individual cells added to give the matrix element $(\mathbf{R})_{ij}$. For the reduced set of (3.66), the key integrations required for all directions are,

$$\begin{aligned} I_1 &= \int_j^{j+1} P_j^2(q) dq = 1 \\ I_2 &= \int_j^{j+1} \chi_j^2(q) dq = \frac{1}{3} \\ I_3 &= \int_j^{j+1} P_j(q)\chi_j(q) dq = \frac{1}{2} \end{aligned} \quad (3.70)$$

and the derived integrals from (3.70) are,

$$\begin{aligned} I_4 &= \int_j^{j+1} (P_j(q) - \chi_j(q))^2 dq = \frac{1}{3} \\ I_5 &= \int_j^{j+1} \chi_j(q)(P_j(q) - \chi_j(q)) dq = \frac{1}{6} \end{aligned} \quad (3.71)$$

Note that $(\mathbf{R})_{ij} = (\mathbf{R})_{ji}$. Also note that we only need to find the interaction of local edges 1 to 4 with local edges 1 to 8 analytically and the rest can be done by just rotation of the x, y and z components. Hence, the minimum terms that are required are,

$$\int_{V_{klm}} \nabla \times \mathbf{N}^{(x)}_{1,\,klm}(\mathbf{r}) \cdot \nabla \times \mathbf{N}^{(x)}_{1,\,klm}(\mathbf{r}) d\mathbf{r} \;=\; I_1[I_4 I_1 + I_4 I_1] = \frac{2}{3}$$

$$\int_{V_{klm}} \nabla \times \mathbf{N}^{(x)}_{1,\,klm}(\mathbf{r}) \cdot \nabla \times \mathbf{N}^{(x)}_{2,\,klm}(\mathbf{r}) d\mathbf{r} = I_1[I_5 I_1 - I_4 I_1] = -\frac{1}{6}$$
$$\int_{V_{klm}} \nabla \times \mathbf{N}^{(x)}_{1,\,klm}(\mathbf{r}) \cdot \nabla \times \mathbf{N}^{(x)}_{3,\,klm}(\mathbf{r}) d\mathbf{r} = I_1[-I_4 I_1 + I_5 I_1] = -\frac{1}{6}$$
$$\int_{V_{klm}} \nabla \times \mathbf{N}^{(x)}_{1,\,klm}(\mathbf{r}) \cdot \nabla \times \mathbf{N}^{(x)}_{4,\,klm}(\mathbf{r}) d\mathbf{r} = I_1[-I_5 I_1 - I_5 I_1] = -\frac{1}{3}$$
$$\int_{V_{klm}} \nabla \times \mathbf{N}^{(x)}_{1,\,klm}(\mathbf{r}) \cdot \nabla \times \mathbf{N}^{(y)}_{5,\,klm}(\mathbf{r}) d\mathbf{r} = -I_1 I_1 I_4 = -\frac{1}{3}$$
$$\int_{V_{klm}} \nabla \times \mathbf{N}^{(x)}_{1,\,klm}(\mathbf{r}) \cdot \nabla \times \mathbf{N}^{(y)}_{6,\,klm}(\mathbf{r}) d\mathbf{r} = -I_1 I_1 I_5 = -\frac{1}{6}$$
$$\int_{V_{klm}} \nabla \times \mathbf{N}^{(x)}_{1,\,klm}(\mathbf{r}) \cdot \nabla \times \mathbf{N}^{(y)}_{7,\,klm}(\mathbf{r}) d\mathbf{r} = I_1 I_1 I_4 = \frac{1}{3}$$
$$\int_{V_{klm}} \nabla \times \mathbf{N}^{(x)}_{1,\,klm}(\mathbf{r}) \cdot \nabla \times \mathbf{N}^{(y)}_{8,\,klm}(\mathbf{r}) d\mathbf{r} = I_1 I_1 I_5 = \frac{1}{6}$$

$$\int_{V_{klm}} \nabla \times \mathbf{N}^{(x)}_{2,\,klm}(\mathbf{r}) \cdot \nabla \times \mathbf{N}^{(x)}_{2,\,klm}(\mathbf{r}) d\mathbf{r} = I_1[I_2 I_1 + I_4 I_1] = \frac{2}{3}$$
$$\int_{V_{klm}} \nabla \times \mathbf{N}^{(x)}_{2,\,klm}(\mathbf{r}) \cdot \nabla \times \mathbf{N}^{(x)}_{3,\,klm}(\mathbf{r}) d\mathbf{r} = I_1[-I_5 I_1 - I_5 I_1] = -\frac{1}{3}$$
$$\int_{V_{klm}} \nabla \times \mathbf{N}^{(x)}_{2,\,klm}(\mathbf{r}) \cdot \nabla \times \mathbf{N}^{(x)}_{4,\,klm}(\mathbf{r}) d\mathbf{r} = I_1[-I_2 I_1 + I_5 I_1] = -\frac{1}{3}$$
$$\int_{V_{klm}} \nabla \times \mathbf{N}^{(x)}_{2,\,klm}(\mathbf{r}) \cdot \nabla \times \mathbf{N}^{(y)}_{5,\,klm}(\mathbf{r}) d\mathbf{r} = I_1 I_1 I_4 = \frac{1}{3}$$
$$\int_{V_{klm}} \nabla \times \mathbf{N}^{(x)}_{2,\,klm}(\mathbf{r}) \cdot \nabla \times \mathbf{N}^{(y)}_{6,\,klm}(\mathbf{r}) d\mathbf{r} = I_1 I_1 I_5 = \frac{1}{6}$$
$$\int_{V_{klm}} \nabla \times \mathbf{N}^{(x)}_{2,\,klm}(\mathbf{r}) \cdot \nabla \times \mathbf{N}^{(y)}_{7,\,klm}(\mathbf{r}) d\mathbf{r} = -I_1 I_1 I_4 = -\frac{1}{3}$$
$$\int_{V_{klm}} \nabla \times \mathbf{N}^{(x)}_{2,\,klm}(\mathbf{r}) \cdot \nabla \times \mathbf{N}^{(y)}_{8,\,klm}(\mathbf{r}) d\mathbf{r} = -I_1 I_1 I_5 = -\frac{1}{6}$$

$$\int_{V_{klm}} \nabla \times \mathbf{N}^{(x)}_{3,\,klm}(\mathbf{r}) \cdot \nabla \times \mathbf{N}^{(x)}_{3,\,klm}(\mathbf{r}) d\mathbf{r} = I_1[I_4 I_1 + I_2 I_1] = \frac{2}{3}$$
$$\int_{V_{klm}} \nabla \times \mathbf{N}^{(x)}_{3,\,klm}(\mathbf{r}) \cdot \nabla \times \mathbf{N}^{(x)}_{4,\,klm}(\mathbf{r}) d\mathbf{r} = I_1[I_5 I_1 - I_2 I_1] = -\frac{1}{6}$$
$$\int_{V_{klm}} \nabla \times \mathbf{N}^{(x)}_{3,\,klm}(\mathbf{r}) \cdot \nabla \times \mathbf{N}^{(y)}_{5,\,klm}(\mathbf{r}) d\mathbf{r} = -I_1 I_1 I_5 = -\frac{1}{6}$$
$$\int_{V_{klm}} \nabla \times \mathbf{N}^{(x)}_{3,\,klm}(\mathbf{r}) \cdot \nabla \times \mathbf{N}^{(y)}_{6,\,klm}(\mathbf{r}) d\mathbf{r} = -I_1 I_1 I_2 = -\frac{1}{3}$$
$$\int_{V_{klm}} \nabla \times \mathbf{N}^{(x)}_{3,\,klm}(\mathbf{r}) \cdot \nabla \times \mathbf{N}^{(y)}_{7,\,klm}(\mathbf{r}) d\mathbf{r} = I_1 I_1 I_5 = \frac{1}{6}$$
$$\int_{V_{klm}} \nabla \times \mathbf{N}^{(x)}_{3,\,klm}(\mathbf{r}) \cdot \nabla \times \mathbf{N}^{(y)}_{8,\,klm}(\mathbf{r}) d\mathbf{r} = I_1 I_1 I_2 = \frac{1}{3}$$

$$\begin{aligned}
\int_{V_{klm}} \nabla \times \mathbf{N}^{(x)}_{4,\,klm}(\mathbf{r}) \cdot \nabla \times \mathbf{N}^{(x)}_{4,\,klm}(\mathbf{r}) d\mathbf{r} &= I_1[I_2 I_1 + I_2 I_1] = \frac{2}{3} \\
\int_{V_{klm}} \nabla \times \mathbf{N}^{(x)}_{4,\,klm}(\mathbf{r}) \cdot \nabla \times \mathbf{N}^{(y)}_{5,\,klm}(\mathbf{r}) d\mathbf{r} &= I_1 I_1 I_5 = \frac{1}{6} \\
\int_{V_{klm}} \nabla \times \mathbf{N}^{(x)}_{4,\,klm}(\mathbf{r}) \cdot \nabla \times \mathbf{N}^{(y)}_{6,\,klm}(\mathbf{r}) d\mathbf{r} &= I_1 I_1 I_2 = \frac{1}{3} \\
\int_{V_{klm}} \nabla \times \mathbf{N}^{(x)}_{4,\,klm}(\mathbf{r}) \cdot \nabla \times \mathbf{N}^{(y)}_{7,\,klm}(\mathbf{r}) d\mathbf{r} &= -I_1 I_1 I_5 = -\frac{1}{6} \\
\int_{V_{klm}} \nabla \times \mathbf{N}^{(x)}_{4,\,klm}(\mathbf{r}) \cdot \nabla \times \mathbf{N}^{(y)}_{8,\,klm}(\mathbf{r}) d\mathbf{r} &= -I_1 I_1 I_2 = -\frac{1}{3}
\end{aligned} \tag{3.72}$$

Using these integral we can evaluate $(\mathbf{R})_{ij}$ as

$$(\mathbf{R})_{ij} = \frac{1}{\sigma_0 - \sigma_f} \sum_{\epsilon} \sum_{\epsilon'} \int_{V_{klm}} \nabla \times \mathbf{N}^{(x)}_{\epsilon,\,klm}(\mathbf{r}) \cdot \nabla \times \mathbf{N}^{(x)}_{\epsilon',\,klm}(\mathbf{r}) d\mathbf{r} \tag{3.73}$$

where ϵ and ϵ' $(\epsilon, \epsilon' = 1, 2, \ldots 12)$ are the local edge indices for the ith and jth global mesh edges.

3.3.2.3 Computation of $\mathbf{L}_0^V$ Matrix Terms

Computation of $(\mathbf{L}_0^V)_{ij}$ can be reduced to a point matching scheme where the basis function caluclated from a correlation integral and the testing function is a delta function as expressed in (3.42). Therefore, we are required to find the correlation function associated with each direction. Using the notation,

$$[\phi_0 \circ \psi_J](q) = \int \phi_0(q + q')\psi_J(q')dq' \tag{3.74}$$

where '$\circ$' represents the correlation, we can define the key correlation functions that are involved as,

Case I

$$C_J^1(q) = [P_0 \circ \chi_J](q) = \begin{cases} C_J^{11}(q), & \text{for } J - 1 \leq q < J \\ C_J^{12}(q), & \text{for } J \leq q < J + 1 \\ 0, & \text{otherwise} \end{cases} \tag{3.75}$$

where,

$$\begin{aligned} C_J^{11}(q) &= \int_{J-q}^{1} (x' + q - J)dx' \\ &= \frac{1}{2} - J + \frac{J^2}{2} + q - Jq + \frac{q^2}{2} \\ C_J^{12}(q) &= \int_{0}^{J+1-q} (x' + q - J)dx' \\ &= \frac{1}{2} - \frac{J^2}{2} + Jq - \frac{q^2}{2} \end{aligned} \tag{3.76}$$

Since,

$$\int_{-\infty}^{\infty} P_{j,0}(x)P_{i,K}(x+q)dx = \int_{-\infty}^{\infty} P_{i,0}(x)P_{j,-K}(x-q)dx \tag{3.77}$$

therefore, we can write

$$(\chi_0 \circ P_J)(q) = C_{-J}^{1}(-q) \tag{3.78}$$

As the correlation term is normalized with respect to l_q, therefore, we will have a factor of l_q while computing L_0^V. A similar analysis is also done for other key correlation terms.

Case II

$$C_J^2(q) = [\chi_0 \circ \chi_J](q) = \begin{cases} C_J^{21}(q), & \text{for } J-1 \leq q < J \\ C_J^{22}, & \text{for } J \leq q < J+1 \\ 0, & \text{otherwise} \end{cases} \tag{3.79}$$

where,

$$\begin{aligned} C_J^{21}(q) &= \int_{J-q}^{1} x'(x' + q - J)dx' \\ &= \frac{1}{3} - \frac{J}{2} + \frac{J^3}{6} + \frac{q}{2} - \frac{J^2 q}{2} + \frac{Jq^2}{2} - \frac{q^3}{6} \\ C_J^{22}(q) &= \int_{0}^{J+1-q} x'(x' + q - J)dx' \qquad (3.80) \\ &= \frac{1}{3} + \frac{J}{2} - \frac{J^3}{6} - \frac{q}{2} + \frac{J^2 q}{2} - \frac{Jq^2}{2} + \frac{q^3}{6} \qquad (3.81) \end{aligned}$$

This function has a symmetry around $q = J$.

Case III

$$C_J^3(q) = [P_0 \circ P_J](q) = \begin{cases} (q+1-J), & \text{for } J-1 \le q < J \\ (1+J-q), & \text{for } J \le q < J+1 \\ 0, & \text{otherwise} \end{cases} \tag{3.82}$$

We can also write equation (3.82) as,

$$C_J^3(q) = \chi_{J-1}(q) + P_J(q) - \chi_J(q) \tag{3.83}$$

This function has a symmetry around $q = J$. And the derived correlation functions are,

$$\begin{aligned} C_J^4(q) &= [(P_0 - \chi_0) \circ (P_J - \chi_J)](q) = C_J^3(q) - C_{-J}^1(-q) - C_J^1(q) + C_J^2(q) \\ C_J^5(q) &= [(P_0 - \chi_0) \circ \chi_J](q) = C_J^1(q) - C_J^2(q) \\ C_J^6(q) &= [\chi_0 \circ (P_J - \chi_J)](q) = C_{-J}^1(-q) - C_J^2(q) \end{aligned} \tag{3.84}$$

As the $\nabla \times \mathbf{N}_e$ for local edge numbers 5 to 8 are just the rotation of x, y and z in the local edge numbers 1 to 4 in addition to interchanging $C_J^5(q)$ and $C_J^6(q)$ with each other. Therefore, we only need to find the correlation functions associated with the interaction of edges 1 to 4 with all of 8 edges of the other cell. Here also $(\mathbf{L}_0^V)_{ij} = (\mathbf{L}_0^V)_{ji}$ as in the case of $\mathbf{R}$ matrix. The minimum terms that are required,

$$\begin{aligned}
\int_{\Omega_{klm}} \nabla \times \mathbf{N}_{1,000}^{(x)}(\mathbf{r}') \cdot \nabla \times \mathbf{N}_{1,klm}^{(x)}(\mathbf{r}+\mathbf{r}')d\mathbf{r}' &= C_k^3(x)[C_l^4(y)C_m^3(z) + C_m^4(z)C_l^3(y)] \\
\int_{\Omega_{klm}} \nabla \times \mathbf{N}_{1,000}^{(x)}(\mathbf{r}') \cdot \nabla \times \mathbf{N}_{2,klm}^{(x)}(\mathbf{r}+\mathbf{r}')d\mathbf{r}' &= C_k^3(x)[C_l^5(y)C_m^3(z) - C_m^4(z)C_l^3(y)] \\
\int_{\Omega_{klm}} \nabla \times \mathbf{N}_{1,000}^{(x)}(\mathbf{r}') \cdot \nabla \times \mathbf{N}_{3,klm}^{(x)}(\mathbf{r}+\mathbf{r}')d\mathbf{r}' &= C_k^3(x)[-C_l^4(y)C_m^3(z) + C_m^5(z)C_l^3(y)] \\
\int_{\Omega_{klm}} \nabla \times \mathbf{N}_{1,000}^{(x)}(\mathbf{r}') \cdot \nabla \times \mathbf{N}_{4,klm}^{(x)}(\mathbf{r}+\mathbf{r}')d\mathbf{r}' &= C_k^3(x)[-C_l^5(y)C_m^3(z) - C_m^5(z)C_l^3(y)] \\
\int_{\Omega_{klm}} \nabla \times \mathbf{N}_{1,000}^{(x)}(\mathbf{r}') \cdot \nabla \times \mathbf{N}_{5,klm}^{(y)}(\mathbf{r}+\mathbf{r}')d\mathbf{r}' &= -C_k^3(x)C_l^3(y)C_m^4(z) \\
\int_{\Omega_{klm}} \nabla \times \mathbf{N}_{1,000}^{(x)}(\mathbf{r}') \cdot \nabla \times \mathbf{N}_{6,klm}^{(y)}(\mathbf{r}+\mathbf{r}')d\mathbf{r}' &= -C_k^3(x)C_l^3(y)C_m^5(z) \\
\int_{\Omega_{klm}} \nabla \times \mathbf{N}_{1,000}^{(x)}(\mathbf{r}') \cdot \nabla \times \mathbf{N}_{7,klm}^{(y)}(\mathbf{r}+\mathbf{r}')d\mathbf{r}' &= C_k^3(x)C_l^3(y)C_m^4(z) \\
\int_{\Omega_{klm}} \nabla \times \mathbf{N}_{1,000}^{(x)}(\mathbf{r}') \cdot \nabla \times \mathbf{N}_{8,klm}^{(y)}(\mathbf{r}+\mathbf{r}')d\mathbf{r}' &= C_k^3(x)C_l^3(y)C_m^5(z)
\end{aligned}$$

$$\int_{\Omega_{klm}} \nabla \times \mathbf{N}^{(x)}_{2,000}(\mathbf{r}') \cdot \nabla \times \mathbf{N}^{(x)}_{1,klm}(\mathbf{r}+\mathbf{r}')d\mathbf{r}' = C^3_k(x)[C^6_l(y)C^3_m(z) - C^4_m(z)C^3_l(y)]$$
$$\int_{\Omega_{klm}} \nabla \times \mathbf{N}^{(x)}_{2,000}(\mathbf{r}') \cdot \nabla \times \mathbf{N}^{(x)}_{2,klm}(\mathbf{r}+\mathbf{r}')d\mathbf{r}' = C^3_k(x)[C^2_l(y)C^3_m(z) + C^4_m(z)C^3_l(y)]$$
$$\int_{\Omega_{klm}} \nabla \times \mathbf{N}^{(x)}_{2,000}(\mathbf{r}') \cdot \nabla \times \mathbf{N}^{(x)}_{3,klm}(\mathbf{r}+\mathbf{r}')d\mathbf{r}' = C^3_k(x)[-C^6_l(y)C^3_m(z) - C^5_m(z)C^3_l(y)]$$
$$\int_{\Omega_{klm}} \nabla \times \mathbf{N}^{(x)}_{2,000}(\mathbf{r}') \cdot \nabla \times \mathbf{N}^{(x)}_{4,klm}(\mathbf{r}+\mathbf{r}')d\mathbf{r}' = C^3_k(x)[-C^2_l(y)C^3_m(z) + C^5_m(z)C^3_l(y)]$$
$$\int_{\Omega_{klm}} \nabla \times \mathbf{N}^{(x)}_{2,000}(\mathbf{r}') \cdot \nabla \times \mathbf{N}^{(y)}_{5,klm}(\mathbf{r}+\mathbf{r}')d\mathbf{r}' = C^3_k(x)C^3_l(y)C^4_m(z)$$
$$\int_{\Omega_{klm}} \nabla \times \mathbf{N}^{(x)}_{2,000}(\mathbf{r}') \cdot \nabla \times \mathbf{N}^{(y)}_{6,klm}(\mathbf{r}+\mathbf{r}')d\mathbf{r}' = C^3_k(x)C^3_l(y)C^5_m(z)$$
$$\int_{\Omega_{klm}} \nabla \times \mathbf{N}^{(x)}_{2,000}(\mathbf{r}') \cdot \nabla \times \mathbf{N}^{(y)}_{7,klm}(\mathbf{r}+\mathbf{r}')d\mathbf{r}' = -C^3_k(x)C^3_l(y)C^4_m(z)$$
$$\int_{\Omega_{klm}} \nabla \times \mathbf{N}^{(x)}_{2,000}(\mathbf{r}') \cdot \nabla \times \mathbf{N}^{(y)}_{8,klm}(\mathbf{r}+\mathbf{r}')d\mathbf{r}' = -C^3_k(x)C^3_l(y)C^5_m(z)$$

$$\int_{\Omega_{klm}} \nabla \times \mathbf{N}^{(x)}_{3,000}(\mathbf{r}') \cdot \nabla \times \mathbf{N}^{(x)}_{1,klm}(\mathbf{r}+\mathbf{r}')d\mathbf{r}' = C^3_k(x)[-C^4_l(y)C^3_m(z) + C^6_m(z)C^3_l(y)]$$
$$\int_{\Omega_{klm}} \nabla \times \mathbf{N}^{(x)}_{3,000}(\mathbf{r}') \cdot \nabla \times \mathbf{N}^{(x)}_{2,klm}(\mathbf{r}+\mathbf{r}')d\mathbf{r}' = C^3_k(x)[-C^5_l(y)C^3_m(z) - C^6_m(z)C^3_l(y)]$$
$$\int_{\Omega_{klm}} \nabla \times \mathbf{N}^{(x)}_{3,000}(\mathbf{r}') \cdot \nabla \times \mathbf{N}^{(x)}_{3,klm}(\mathbf{r}+\mathbf{r}')d\mathbf{r}' = C^3_k(x)[C^4_l(y)C^3_m(z) + C^2_m(z)C^3_l(y)]$$
$$\int_{\Omega_{klm}} \nabla \times \mathbf{N}^{(x)}_{3,000}(\mathbf{r}') \cdot \nabla \times \mathbf{N}^{(x)}_{4,klm}(\mathbf{r}+\mathbf{r}')d\mathbf{r}' = C^3_k(x)[C^5_l(y)C^3_m(z) - C^2_m(z)C^3_l(y)]$$
$$\int_{\Omega_{klm}} \nabla \times \mathbf{N}^{(x)}_{3,000}(\mathbf{r}') \cdot \nabla \times \mathbf{N}^{(y)}_{5,klm}(\mathbf{r}+\mathbf{r}')d\mathbf{r}' = -C^3_k(x)C^3_l(y)C^6_m(z)$$
$$\int_{\Omega_{klm}} \nabla \times \mathbf{N}^{(x)}_{3,000}(\mathbf{r}') \cdot \nabla \times \mathbf{N}^{(y)}_{6,klm}(\mathbf{r}+\mathbf{r}')d\mathbf{r}' = -C^3_k(x)C^3_l(y)C^2_m(z)$$
$$\int_{\Omega_{klm}} \nabla \times \mathbf{N}^{(x)}_{3,000}(\mathbf{r}') \cdot \nabla \times \mathbf{N}^{(y)}_{7,klm}(\mathbf{r}+\mathbf{r}')d\mathbf{r}' = C^3_k(x)C^3_l(y)C^6_m(z)$$
$$\int_{\Omega_{klm}} \nabla \times \mathbf{N}^{(x)}_{3,000}(\mathbf{r}') \cdot \nabla \times \mathbf{N}^{(y)}_{8,klm}(\mathbf{r}+\mathbf{r}')d\mathbf{r}' = C^3_k(x)C^3_l(y)C^2_m(z)$$

$$\int_{\Omega_{klm}} \nabla \times \mathbf{N}^{(x)}_{4,000}(\mathbf{r}') \cdot \nabla \times \mathbf{N}^{(x)}_{1,klm}(\mathbf{r}+\mathbf{r}')d\mathbf{r}' = C^3_k(x)[-C^6_l(y)C^3_m(z) - C^6_m(z)C^3_l(y)]$$
$$\int_{\Omega_{klm}} \nabla \times \mathbf{N}^{(x)}_{4,000}(\mathbf{r}') \cdot \nabla \times \mathbf{N}^{(x)}_{2,klm}(\mathbf{r}+\mathbf{r}')d\mathbf{r}' = C^3_k(x)[-C^2_l(y)C^3_m(z) + C^6_m(z)C^3_l(y)]$$
$$\int_{\Omega_{klm}} \nabla \times \mathbf{N}^{(x)}_{4,000}(\mathbf{r}') \cdot \nabla \times \mathbf{N}^{(x)}_{3,klm}(\mathbf{r}+\mathbf{r}')d\mathbf{r}' = C^3_k(x)[C^6_l(y)C^3_m(z) - C^2_m(z)C^3_l(y)]$$
$$\int_{\Omega_{klm}} \nabla \times \mathbf{N}^{(x)}_{4,000}(\mathbf{r}') \cdot \nabla \times \mathbf{N}^{(x)}_{4,klm}(\mathbf{r}+\mathbf{r}')d\mathbf{r}' = C^3_k(x)[C^2_l(y)C^3_m(z) + C^2_m(z)C^3_l(y)]$$

$$\begin{aligned}
\int_{\Omega_{klm}} \nabla \times \mathbf{N}^{(x)}_{4,000}(\mathbf{r}') \cdot \nabla \times \mathbf{N}^{(y)}_{5,klm}(\mathbf{r}+\mathbf{r}')d\mathbf{r}' &= C^3_k(x)C^3_l(y)C^6_m(z) \\
\int_{\Omega_{klm}} \nabla \times \mathbf{N}^{(x)}_{4,000}(\mathbf{r}') \cdot \nabla \times \mathbf{N}^{(y)}_{6,klm}(\mathbf{r}+\mathbf{r}')d\mathbf{r}' &= C^3_k(x)C^3_l(y)C^2_m(z) \\
\int_{\Omega_{klm}} \nabla \times \mathbf{N}^{(x)}_{4,000}(\mathbf{r}') \cdot \nabla \times \mathbf{N}^{(y)}_{7,klm}(\mathbf{r}+\mathbf{r}')d\mathbf{r}' &= -C^3_k(x)C^3_l(y)C^6_m(z) \\
\int_{\Omega_{klm}} \nabla \times \mathbf{N}^{(x)}_{4,000}(\mathbf{r}') \cdot \nabla \times \mathbf{N}^{(y)}_{8,klm}(\mathbf{r}+\mathbf{r}')d\mathbf{r}' &= -C^3_k(x)C^3_l(y)C^2_m(z) \qquad (3.85)
\end{aligned}$$

All these terms are in normalized coordinate system, hence while computing $\mathbf{L}^0_V$ we will have factor of V_0, i.e. the volume of the discretization cell. The integration of correlation function along with scalar Green's function of (3.18) can be preformed numerically by again taking few fixed points in a cell. As the correlation functions have zero value at the surface of its defining cell, therefore, we can subdivide the cell into smaller parts, typically x^3 where $x = 2, 4, 6 \ldots$,and use the same volume integration scheme as described in the computation of $\mathbf{V}^0$ matrix. For self interacting cells we will have singularity present in the Green's function which can be dealt analytically. For self interacting cells we can divide the Green's function of (3.18) into two parts as,

$$G_0(\mathbf{r}|\mathbf{r}') = \frac{e^{ik|\mathbf{r}-\mathbf{r}'|}}{4\pi|\mathbf{r}-\mathbf{r}'|} = \frac{ik}{4\pi}\text{sinc}\left(\frac{ik|\mathbf{r}-\mathbf{r}'|}{2}\right)e^{\frac{ik|\mathbf{r}-\mathbf{r}'|}{2}} + \frac{1}{4\pi|\mathbf{r}-\mathbf{r}'|} \qquad (3.86)$$

The first part is now can be computed numerically as it doesn't contain any more singularity. For the later part, which is the singular part, we notice that in general the correlation function has a form of linear in x, cubic in y and linear again in z or linear in x, cubic in z and linear again in y for (3.85). For correlation function with linear in x, cubic in y and linear in z, we can write

$$\begin{aligned}
\beta(x,y,z) = C^3_k(x)C^i_l(y)C^3_m(z) &= a_0 + a_1 z + a_2 y + a_3 yz + a_4 y^2 + a_5 y^2 z + a_6 y^3 + a_7 y^3 z \\
&\quad + a_8 x + a_9 xz + a_{10} xy + a_{11} xyz + a_{12} xy^2 + a_{13} xy^2 z \\
&\quad + a_{14} xy^3 + a_{15} xy^3 z, \text{ where } i = 2 \text{ or } 4 \text{ or } 5 \text{ or } 6 \qquad (3.87)
\end{aligned}$$

a_0 to a_{15} are the constants determined by the correlation functions. For an exclusion zone of $8a^3$ volume centered at origin, we can compute analytical value of the Green's function along with components of (3.87) in each quadrant. For this purpose Mathematica Software is used for finding the analytical results in the first quadrant, O_1, and for the rest of the quadrants we

can use the same value but with proper sign [5]. We only need to define a small set of analytical values as $\int_{O_1} \frac{x}{4\pi|\mathbf{r}|} d\mathbf{r} = \int_{O_1} \frac{y}{4\pi|\mathbf{r}|} d\mathbf{r}$ and similarly others. Hence the required set,

$$\begin{aligned}
p_0 &= \int_{O_1} \frac{1}{4\pi|\mathbf{r}|}\, d\mathbf{r} &= 0.094700a^2 \\
p_1 &= \frac{1}{a}\int_{O_1} \frac{x}{4\pi|\mathbf{r}|}\, d\mathbf{r} &= 0.041030a^2 \\
p_2 &= \frac{1}{a^2}\int_{O_1} \frac{xy}{4\pi|\mathbf{r}|}\, d\mathbf{r} &= 0.018565a^2 \\
p_3 &= \frac{1}{a^3}\int_{O_1} \frac{xyz}{4\pi|\mathbf{r}|}\, d\mathbf{r} &= 0.008583a^2 \\
p_4 &= \frac{1}{a^2}\int_{O_1} \frac{x^2}{4\pi|\mathbf{r}|}\, d\mathbf{r} &= 0.025480a^2 \\
p_5 &= \frac{1}{a^3}\int_{O_1} \frac{x^2y}{4\pi|\mathbf{r}|}\, d\mathbf{r} &= 0.011731a^2 \\
p_6 &= \frac{1}{a^4}\int_{O_1} \frac{x^2yz}{4\pi|\mathbf{r}|}\, d\mathbf{r} &= 0.005478a^2 \\
p_7 &= \frac{1}{a^3}\int_{O_1} \frac{x^3}{4\pi|\mathbf{r}|}\, d\mathbf{r} &= 0.018333a^2 \\
p_8 &= \frac{1}{a^4}\int_{O_1} \frac{x^3y}{4\pi|\mathbf{r}|}\, d\mathbf{r} &= 0.008514a^2 \\
p_9 &= \frac{1}{a^5}\int_{O_1} \frac{x^3yz}{4\pi|\mathbf{r}|}\, d\mathbf{r} &= 0.003998a^2
\end{aligned} \tag{3.88}$$

The region outside the exclusion zone can be computed numerically as described earlier.

3.3.2.4 Computation of $\mathbf{L}_0^S$ Matrix Terms

For $\mathbf{L}_0^S$ matrix, we are looking at the interaction of the edges that are on the flaw-conductor interface only. From (3.66) and (3.31), for a surface directed in $\hat{x}$ direction we will be considering local edges 7 and 8, whereas for $-\hat{x}$ directed it will be local edges 5 and 6, similarly for $\hat{y}$ and $\hat{z}$ directed ones. In general, $\hat{x} \cdot \mathbf{P}_i = \pm P_l(y)P_m(z)$. Here again, as in $\mathbf{L}_0^V$ case, we can reduce reduced (3.66) to a point matching scheme where basis function is a correlation function only in two variables and the testing function is a delta function. Hence we can use the same correlation functions as described in $\mathbf{L}_0^V$ matrix computation. For finding the value numerically, we can express integration in terms of summation of few fixed points [see Eq.

[5] The singularity is an even function in x, y and z and hence the components of (3.87) will determine its sign of the analytical results in different quadrant.

25.4.62, page 892 of (1)] and can handle the singularity exactly in the similar manner. In this case we will have correlation function which will be product of two linear functions, e.g. product of linear in x-direction and y-direction for a surface normal in z-direction. For $\mathbf{L}_0^S$ matrix calculation purpose, the analytical set required will be

$$\begin{aligned} q_0 &= \int_{O_2} \frac{1}{4\pi|\mathbf{r}|}\, d\mathbf{r} &&= 0.140275a \\ q_1 &= \frac{1}{a}\int_{O_2} \frac{x}{4\pi|\mathbf{r}|}\, d\mathbf{r} &&= 0.051550a \\ q_2 &= \frac{1}{a^2}\int_{O_2} \frac{xy}{4\pi|\mathbf{r}|}\, d\mathbf{r} &&= 0.021975a \end{aligned} \tag{3.89}$$

where O_2 is 2D 1st quadrant and $|\mathbf{r}| = \sqrt{x^2+y^2}$ as the singularity is only present when the third variable is zero. Similar to $\mathbf{R}$ and $\mathbf{L}_0^V$, here also we have $(\mathbf{L}_0^S)_{ij} = (\mathbf{L}_0^S)_{ji}$.

3.3.2.5 Computation of $\delta\mathbf{L}$ Matrix Terms for a Half Space Problem

The $\delta\mathcal{G}^{ee}(\mathbf{r}|\mathbf{r}')$ for a half space conductor is given by (3.19) and $V(\mathbf{r}|\mathbf{r}')$ is defined by (3.20). In the case half-space conductor, we have $z+z' > 0$, hence $-$ sign will used in (3.20). In (3.20), L_z is the partial derivative of L with respect to z and L is given by Foster-Lien integral and expressed in terms of Kelvin functions as,

$$L(k,\rho,\zeta) = \int_0^\infty \frac{1}{\gamma} e^{-\gamma\zeta} J_0(\rho s) ds = I_0\left[-\frac{ik}{2}(S-\zeta)\right] K_0\left[-\frac{ik}{2}(S+\zeta)\right] \tag{3.90}$$

where $S^2 = \rho^2 + \zeta^2$ and $\gamma = \sqrt{s^2-k^2}$ with positive real part root (reference chapter 9 of (1)). The partial reflection term can be rewritten as,

$$\frac{1}{k^2}\left[\nabla \times \hat{z}\left[\nabla' \times \hat{z} V(\mathbf{r}|\mathbf{r}')\right]\right] = \frac{1}{k^2}\begin{bmatrix} -\frac{\partial^2 V}{\partial y^2} & \frac{\partial^2 V}{\partial x \partial y} & 0 \\ \frac{\partial^2 V}{\partial x \partial y} & -\frac{\partial^2 V}{\partial x^2} & 0 \\ 0 & 0 & 0 \end{bmatrix} \tag{3.91}$$

A detailed discussion on computing L_{xxz}, L_{yyz} and L_{xyz} using Kelvin functions is given on page 15 of (9). Computation of the image and the transverse electric terms can be reduced to a similar form as that for $\mathbf{L}_0^V$ and $\mathbf{L}_0^S$ in addition to changing the correlation function in z direction to a convolution function. Using the notation,

$$[\phi_0 * \psi_J](q) = \int \phi_0(q-q')\psi_J(q')dq' \tag{3.92}$$

where '$*$' represents the convolution, we can define the key convolution as,

Case I

$$D_J^1(q) = [P_0 * \chi_J](q) = \begin{cases} \frac{1}{2}(J-q)^2, & \text{for } J \leq q < J+1 \\ \frac{1}{2}(-2J - J^2 + 2q + 2Jq - q^2), & \text{for } J+1 \leq q < J+2 \\ 0, & \text{otherwise} \end{cases} \tag{3.93}$$

As its a convolution, therefore, we can write,

$$[P_0 * \chi_J](q) = [\chi_0 * P_J](q) \tag{3.94}$$

Here also the term is normalized with respect to l_q, therefore, we will have a factor of l_q while computing its respective matrix term.

Case II

$$D_J^2(q) = [\chi_0 * \chi_J](q) = \begin{cases} \frac{1}{6}(q-J)^3, & \text{for } J \leq q < J+1 \\ \frac{1}{6}(-4 + J^3 + 6q - 3J^2q - q^3 + 3J(q^2-2)), & \text{for } J+1 \leq q < J+2 \\ 0, & \text{otherwise} \end{cases} \tag{3.95}$$

This function has a symmetry around $q = J+1$.

Case III

$$D_J^3(q) = [P_0 * P_J](q) = \begin{cases} (q-J), & \text{for } J \leq q < J+1 \\ (2+J-q), & \text{for } J+1 \leq q < J+2 \\ 0, & \text{otherwise} \end{cases} \tag{3.96}$$

This function has a symmetry around $q = J+1$. And the derived convolution functions are,

$$\begin{aligned} D_J^4(q) &= [(P_0 - \chi_0) * (P_J - \chi_J)](q) = D_J^3(q) - 2D_J^1(q) + D^2(q) \\ D_J^5(q) &= [(P_0 - \chi_0) * \chi_J](q) = D_J^1(q) - D^2(q) \end{aligned} \tag{3.97}$$

Using these convolution terms and previously defined correlation functions we can also compute the partial reflection terms. In partial reflection terms we only need to consider the $\hat{x}$ or $\hat{y}$ directed components of the (3.66) and the double partial derivatives of $G_0(\mathbf{r}|\mathbf{r}' - 2\hat{z}z')$ are,

$$\frac{\partial^2 G_0(\mathbf{r}|\mathbf{r}' - 2\hat{z}z')}{\partial x^2} = \frac{e^{ikR}}{4\pi R^2}\left[\frac{3}{R^3}(x-x')^2 - \frac{3ik}{R^2}(x-x')^2 - \frac{1}{R} - \frac{k^2}{R}(x-x')^2 + ik\right] \tag{3.98}$$

and

$$\frac{\partial^2 G_0(\mathbf{r}|\mathbf{r}' - 2\hat{z}z')}{\partial x \partial y} = \frac{e^{ikR}}{4\pi R^3}\left[\frac{3}{R^2} - \frac{3ik}{R} - k^2\right](x-x')(y-y') \tag{3.99}$$

where $R = \sqrt{(x-x')^2 + (y-y')^2 + (z+z')^2}$. Here also we have $(\delta\mathbf{L})_{ij} = (\delta\mathbf{L})_{ji}$.

3.4 RESPONSE DUE TO A MAGNETIC SENSOR

A magnetic field sensor response due to an ideal crack is given in terms of sensor current density $\mathbf{J}_M(\mathbf{r})$ and the scattered electric field $\mathbf{E}^{(s)}(\mathbf{r})$,

$$\Delta H = -\int_{Coil} \mathbf{E}^{(s)}(\mathbf{r}) \cdot \mathbf{J}_M(\mathbf{r}) d\mathbf{r} \tag{3.100}$$

where the integration is performed over the coil region. By using reciprocity principle (22) and (9), we can rewrite (3.100) in terms of incident field of the magnetic sensor $\mathbf{E}_M^{(0)}(\mathbf{r})$ and the dipole density of the flaw region $\mathbf{P}(\mathbf{r})$ as,

$$\Delta H = -\int_{\Omega_f} \mathbf{E}_M^{(0)}(\mathbf{r}) \cdot \mathbf{P}(\mathbf{r}) d\mathbf{r} \tag{3.101}$$

From (3.11) and (3.101),

$$\Delta H = -\sum_{e=1}^{E} U_e \int_{\Omega_f} \mathbf{E}_M^{(0)}(\mathbf{r}) \cdot \nabla \times \mathbf{N}_e d\mathbf{r} \tag{3.102}$$

The integral of (3.102) can be solved in the similar manner as that for finding the terms of $\mathbf{V}^{(0)}$ and the unknowns, U_e, are computed from (3.12). As $\mathbf{V}^{(0)}$ matrix values depend upon the position of the excitation coil as the incident electric field changes, therefore, the unknown matrix of $\mathbf{U}$ will also be a function of the probe position. But the rest of the matrixes, on the left hand side of (3.12)are independent of the probe position. Hence for finding the unknowns, its best to find the inverse of the left hand side matrix first and then update the unknown values with respect to new probe position. For this purpose a LU decomposition technique, chapter 2 of (29), is used for finding the solution of the unknowns.

3.5 RESULTS

An example of sensor response to an ideal crack inside a half-space conductor is presented, 3.3. Crack of dimensions 3mm x 3mm x 3mm is assumed. Other related dimensions are listed in Table 3.1. A comparison is made for the same crack between the results of the magnetic sensor with the new code (using edge shaped basis functions) with that of the old code (using point matching scheme). Fig. (3.4) shows the magnitude and phase of the vertical magnetic field at the the center sensor due to the ideal crack. From Fig. (3.4), we can clearly see that we have a good match between the phase of the magnetic sensor from the new code and with that of the old code. On the other hand, we don't have a match between the magnitude plot. This can be due to the problem of not finding correct results of the analytical solution of the singularity in the case of $\mathbf{L}_0^V$ matrix.

3.6 CONCLUSIONS

A theory has been developed for modelling of the flaw region using edge element shaped based basis functions for a magnetic sensor response. Dipole density due to the excitation coil is represented in terms of the new basis function and the dipole densities are found by the use of electric field integral equation. The use of edge element shaped basis function guarantee the zero divergence property of the dipole density inside the flaw region. The equation has been approximated using moment method and a Tree-Cotree decomposition is used to reduce the size of the matrix equation. The solution of the matrix equation is found by using LU decomposition technique. Its application is looked for a problem of an ideal crack in a half-space conductor problem. Based on the theory, a computer simulation code has been written and test for the above problem and the results are compared with the older technique of point matching. The results show a good match between the phase found by the new technique and the old technique. But some issues regarding the magnitude has yet to be solved. The technique looks promising for modelling complex geometries. Tetrahedral modelling will be more useful in the flaw discretization of complex geometries as compared to using parallelepiped division.

Table 3.1 Test parameters for magnetic sensor measurements for a circular coil excitation.

Coil			
Outer radius	3.89 mm	Inner radius	1.55 mm
Axial length	5.99 mm	Nominal lift-off	2.5825 mm
Number of turns	517 ± 1 mm	Number of sensors	33
Height of sensors	0.869 mm	Distance between sensors	2.0 mm
Coil Current	1.0 Amp	Frequency	2000 Hz
Plate			
Conductivity	1.82×10^7 S/m	Flaw Depth	4.85 mm

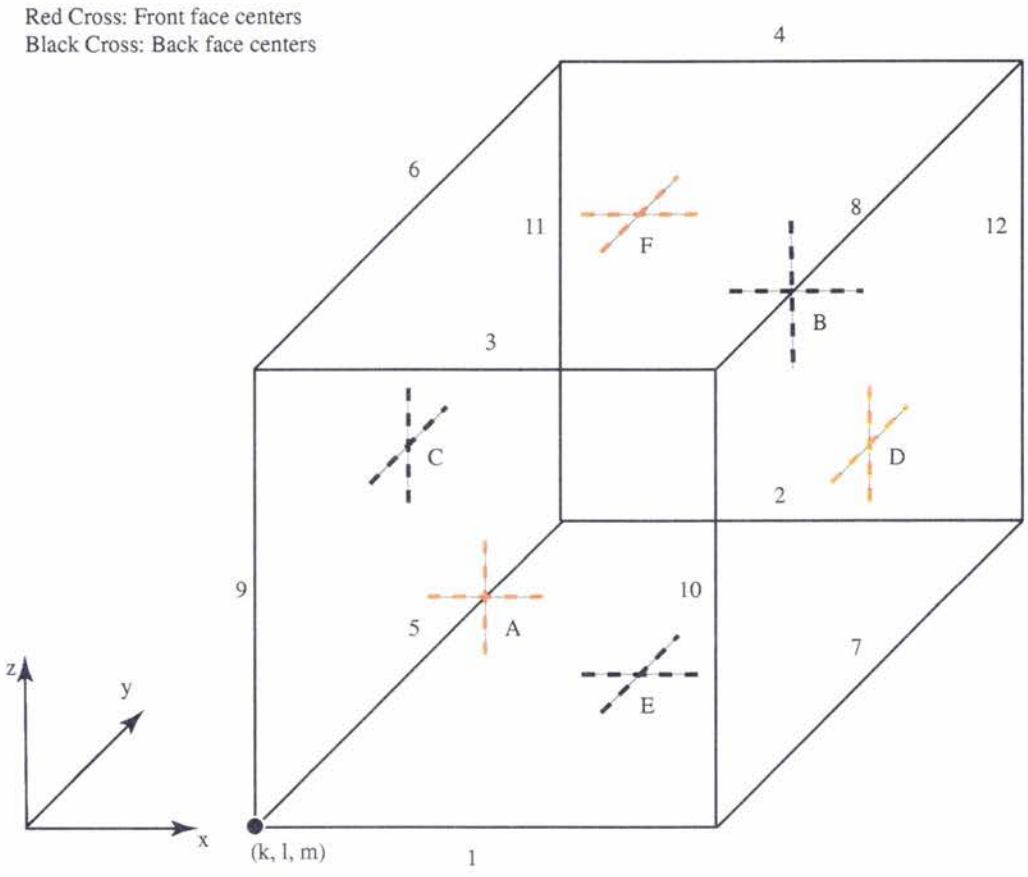

Figure 3.1 Local edge numbering for a parallelepiped at (k, l, m) showing face centers (A to F).

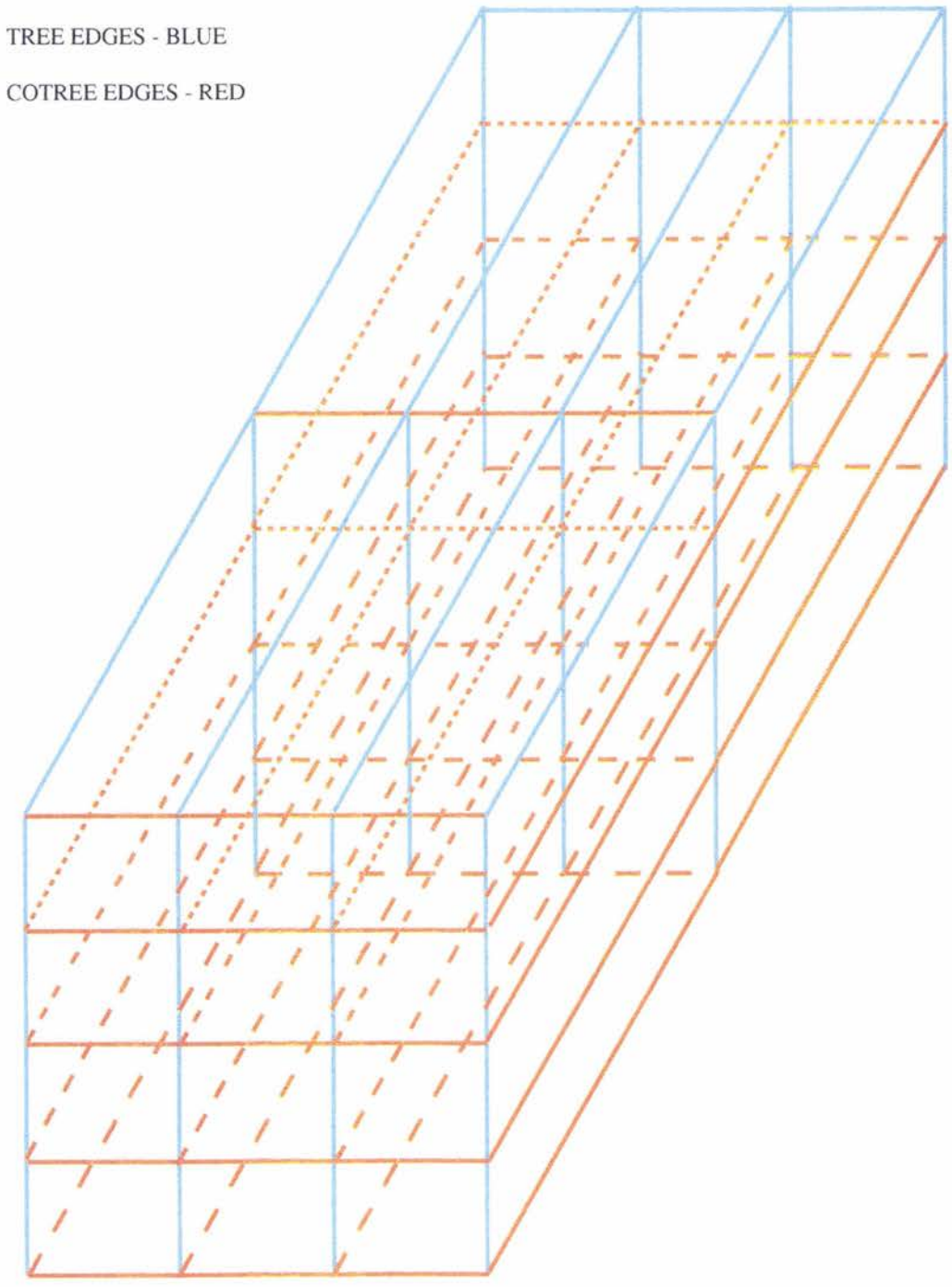

Figure 3.2 Tree-Cotree decomposition.

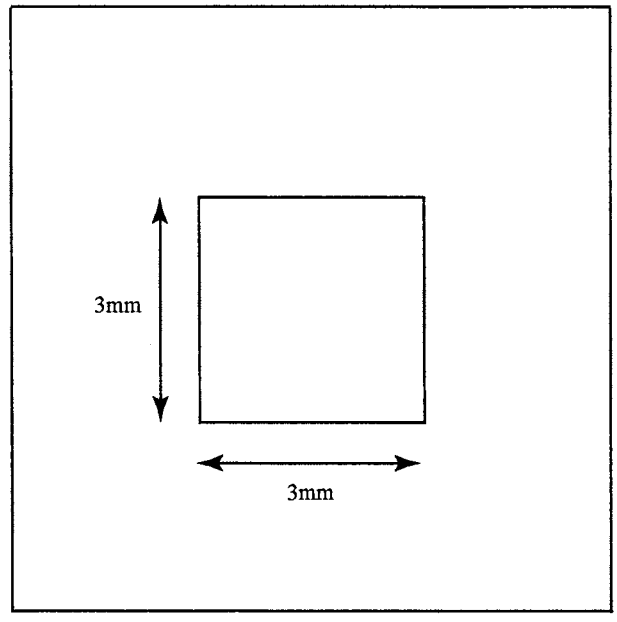

(a) Top View

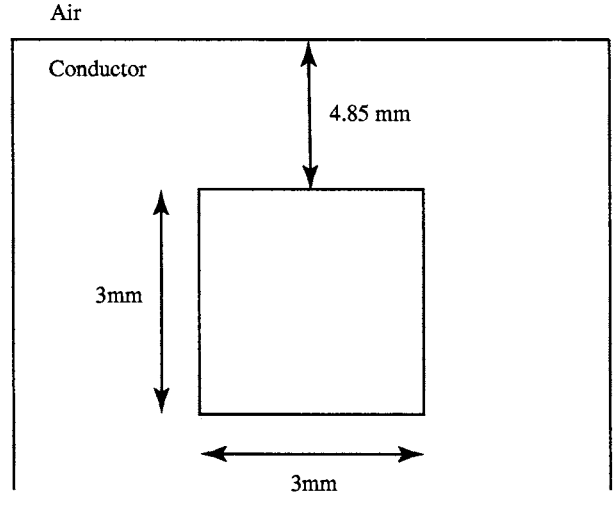

(b) Side View

Figure 3.3 Half space conductor showing a volumetric recess of dimension 3mm x 3mm x 3mm at 4.85mm from the conductor-air surface.

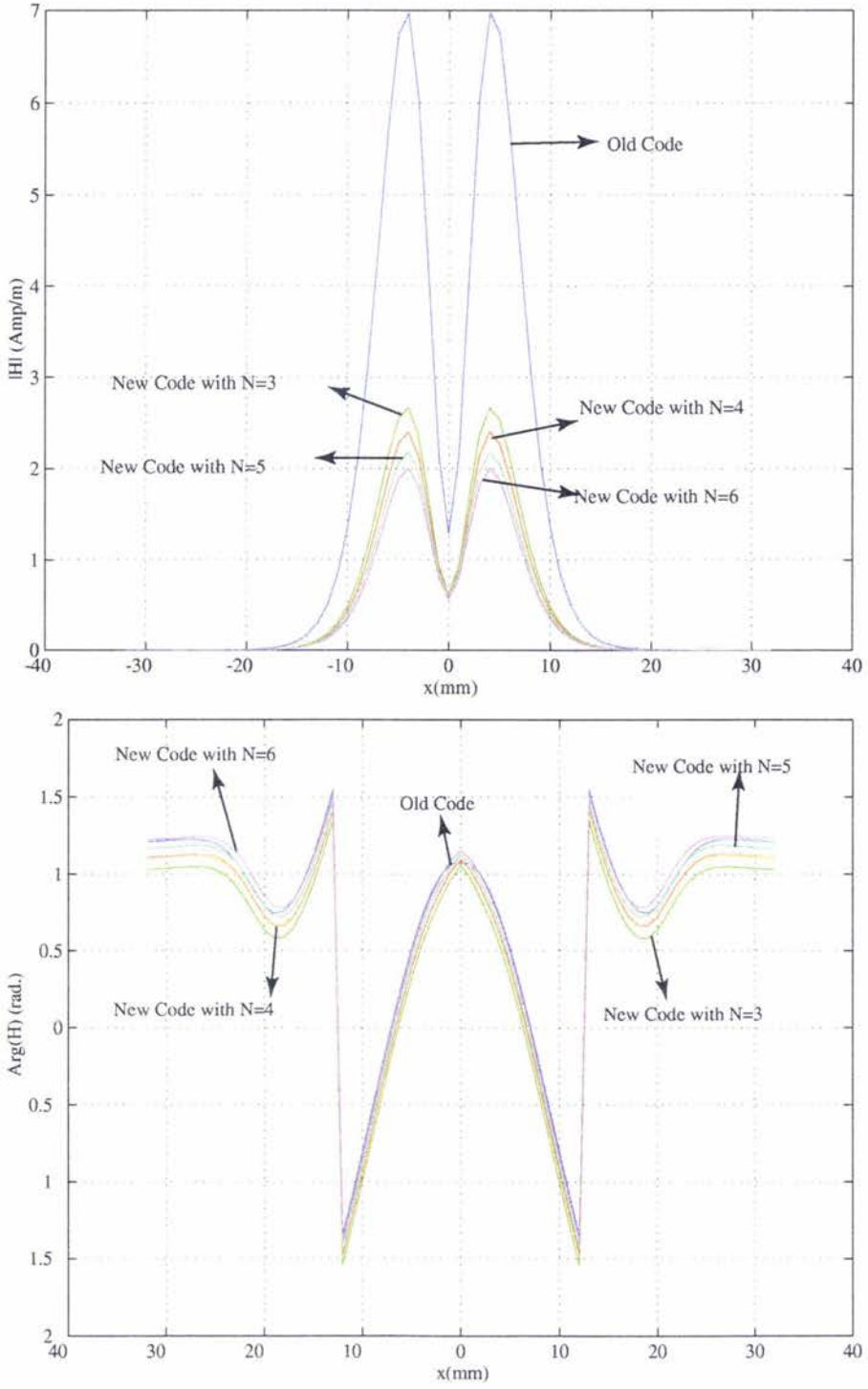

Figure 3.4 Magnitude and phase of the magnetic field for one sensor at the center of the excitation coil. The N in the figure for the new code results indicates that the flaw discretization is NxNxN. Comparison between old code and new code is shown. The discretization of 3x3x3 is done for the old code.

CHAPTER 4. SUMMARY AND DISCUSSION

4.1 GENERAL DISCUSSION

The purpose of this study was to investigate different aspects of the crack characterization using eddy current methods. The first part dealt with the modelling of a new type of coil, a racetrack coil, along with multi sensors scheme, which is needed for a faster scan of a given surface, and the second part was devoted to flaw modelling using a new basis function, edge element shaped basis function, for better convergence to the solution.

The theory of the racetrack coil, in presence of a stratified conductor, has been divided into two parts. The first part for the two straight parts and the second part for the two separate semicircular bends. The field due to both the parts are formulated based on magnetic dipole representation of the flaw or crack due to the excitation coil. The field due to the straight parts is found using a two dimensional Fourier transform, whereas, the field due to the two semicircular bends is based on integrals containing Bessel functions. A linear array of magnetic sensors are incorporated with the design of the racetrack coil. The linear array of magnetic sensors are parallel to the center line of the racetrack coil. This has an advantage over the use of a single sensor as we can scan a given area in one single sweep which will save the scanning time. The design of the new coil along with the multiple sensors is compact and easy to manipulate. The racetrack simulation results are compared to an older circular coil.

In the second part of the thesis, a new technique for flaw characterization is presented. Edge based basis functions are introduced, as compared to using linear roof hat functions, for the representation of the unknown dipole density inside the flaw or crack region due the excitation coil. The unknown dipole density functions are expanded in terms of the edge element shaped functions and variant of Galerkin method for moment method is applied for

solving the matrix equations. Edge element shaped basis functions satisfies the condition of having a zero divergence of the dipole density inside the flaw or crack region. A Tree-Cotree decomposition is used for reducing the number of unknowns. Use of this new technique is looked for a problem of crack in a half-space conductor.

4.2 RECOMMENDATIONS FOR FUTURE RESEARCH

In the thesis use of edge element shaped basis function is presented. A discretization scheme using parallelepiped is used for modelling a flaw or a crack region is looked at. For any arbitrary shaped flaw, the use of parallelepiped for its discretization will not be that help. Hence, use of some other discretization scheme is needed. One such solution would be use of tetrahedral modelling which can provide a better meshing with that of the flaw region.

APPENDIX A. NUMERICAL SOLUTION FOR $\mathcal{J}_\nu^n(z)$

$\mathcal{J}_\nu^n(z)$ is defined as,

$$\mathcal{J}_\nu^n(z) = \int_0^z x^n J_\nu(x)\, dx \tag{A.1}$$

where $n = 1$ or 2 and $m = 0, 1, 2, 3 \ldots$. Bessel function is defined in terms of summation series as, Eq. 9.1.10 of (2),

$$J_\nu(x) = \left(\frac{x}{2}\right)^\nu \sum_{k=0}^{\infty} \frac{\left(-\frac{1}{4}x^2\right)^k}{k!\,\Gamma(\nu + k + 1)} \tag{A.2}$$

If ν is an integer then,

$$J_\nu(x) = \left(\frac{x}{2}\right)^\nu \sum_{k=0}^{\infty} \frac{\left(-\frac{1}{4}x^2\right)^k}{k!\,(\nu + k)!} \tag{A.3}$$

From (A.1) and (A.3),

$$\mathcal{J}_\nu^n(z) = z^{n+1} \left(\frac{z}{2}\right)^\nu \sum_{k=0}^{\infty} \frac{\left(-\frac{1}{4}z^2\right)^k}{k!\,(\nu + k)!\,(\nu + n + 2k + 1)} \tag{A.4}$$

If the argument of z is small, typically less then 6.0, then we can compute the value of $\mathcal{J}_\nu^n(z)$ numerically by expressing as a summation of a series with the requirement of smaller number of terms need in (A.4). But for larger arguments its difficult to get an accurate result with this method. For large argument of ν we can use a recursive relationship based on recursive relationship for the Eq. 11.3.1 of (2). The generalized equation is,

$$g_{\mu,\nu}(z) = \int^z e^{-p\,t} t^\mu Z_\nu(t) dt \tag{A.5}$$

where $Z_\nu(z)$ represents any of the Bessel functions of the first three kinds or the modified Bessel functions. A recursive relationship of (A.5) is given by Eq. 11.3.6 of (2),

$$a\,(\nu - \mu)\, g_{\mu,\nu+1}(z) = -2\,\nu\, e^{-p\,z} z^\mu Z_\nu(z) - 2\,\nu\, p\, g_{\mu,\nu}(z) + b\,(\mu + \nu)\, g_{\mu,\nu-1}(z) \tag{A.6}$$

where $a = b = 1$ for $Z_\nu(z)$ to be $J_\nu(z)$, Eq. 11.3.2 of (2). For our problem for $p = 0$, we can reduce (A.6) to,

$$(\nu - n)\,\mathcal{J}^n_{\nu+1}(z) = -2\,\nu\,z^n\,J_\nu(z) + (\nu + n)\,\mathcal{J}^n_{\nu-1}(z) \tag{A.7}$$

We can use this recursive relationship for finding the values of $\mathcal{J}^n_\nu(z)$ for $\nu > 3$.[1] For $\nu \leq 3$ and $z \leq 6$ can be solved as describe earlier. For $\nu \leq 3$ and $z > 6$, we can split the integral into two parts. The first part will be the integration from 0 to 6 and second form 6 to z as,

$$\mathcal{J}^n_\nu(z) = \int_0^6 x^n J_\nu(x)\,dx + \int_6^z x^n J_\nu(x)\,dx \tag{A.8}$$

For the second part we can assume that the argument of Bessel function, z, is large and can use Hankel's Asymptotic expansion for the Bessel function, Eq. 9.2.5 of (2),

$$J_\nu(z) = \sqrt{\frac{2}{\pi z}}\,[P(\nu, z)\cos\chi - Q(\nu, z)\sin\chi] \tag{A.9}$$

where $\chi = z - \phi = z - (\frac{\nu}{2} + \frac{1}{4})\pi$ and $P(\nu, z)$ and $Q(\nu, z)$ are given by Eq. 9.2.9 and Eq. 9.2.10 of (2) as,

$$P(\nu, z) \sim 1 - \frac{(\mu - 1)(\mu - 9)}{2!\,(8z)^2} + \frac{(\mu - 1)(\mu - 9)(\mu - 25)(\mu - 49)}{4!\,(8z)^4} - \ldots \tag{A.10}$$

and

$$Q(\nu, z) \sim \frac{\mu - 1}{8z} - \frac{(\mu - 1)(\mu - 9)(\mu - 25)}{3!\,(8z)^3} + \ldots \tag{A.11}$$

where $\mu = 4\nu^2$. Hence, we can express (A.9) as,

$$J_\nu(z) = \sqrt{\frac{2}{\pi z}}\left[\left(p_0 - \frac{p_2}{z^2} + \frac{p_4}{z^4} - \ldots\right)\cos(z - \phi) - \left(\frac{q_1}{z} - \frac{q_3}{z^3} + \ldots\right)\sin(z - \phi)\right] \tag{A.12}$$

where $p_0, p_2, p_4, \ldots$ are the coefficients of the $z^2, z^4, \ldots$ terms of (A.10) and $q_1, q_3, \ldots$ are the coefficients of the $z, z^3, \ldots$ terms of (A.11). Combining (A.12) with the second integral of (A.8), we can write

$$\int_{z_0}^z x^n J_\nu(x)\,dx = \sqrt{\frac{2}{\pi}}\,[(p_0 I_0 - p_2 I_2 + p_4 I_4 - \ldots) - (q_1 I_1 - q_3 I_3 + \ldots)] \tag{A.13}$$

[1] $\nu > 3$ is limited by the fact that we have $n = 1$ or 2.

where $z_0 = 6$ and,[2]

$$\begin{aligned} I_{2m} &= \int_{z_0}^{z} x^{n-2m-\frac{1}{2}} \cos(x-\phi)dx \\ I_{2m+1} &= \int_{z_0}^{z} x^{n-2m-\frac{3}{2}} \sin(x-\phi)dx \end{aligned} \tag{A.14}$$

We can rewrite (A.14) as,

$$\begin{aligned} I_{2m} &= \int_{0}^{z} x^{n-2m-\frac{1}{2}} \cos(x-\phi)dx - \int_{0}^{z_0} x^{n-2m-\frac{1}{2}} \cos(x-\phi)dx \\ I_{2m+1} &= \int_{0}^{z} x^{n-2m-\frac{3}{2}} \sin(x-\phi)dx - \int_{0}^{z_0} x^{n-2m-\frac{3}{2}} \sin(x-\phi)dx \end{aligned} \tag{A.15}$$

and performing integration by parts we can form a recursive relationship as,

$$\begin{aligned} I_{2m+1} &= \frac{1}{n-2m-\frac{1}{2}} \left[\sin(z-\phi)z^{n-2m-\frac{1}{2}} - \sin(z_0-\phi){z_0}^{n-2m-\frac{1}{2}} - I_{2m}\right] \\ I_{2m} &= \frac{1}{n-2m-\frac{3}{2}} \left[\cos(z-\phi)z^{n-2m-\frac{3}{2}} - \cos(z_0-\phi){z_0}^{n-2m-\frac{3}{2}} + I_{2m-1}\right] \end{aligned} \tag{A.16}$$

Therefore, we can reduce all I_m terms to I_0 form. We can solve I_0 using Fresnel integrals, Eq. 7.3.1 and Eq. 7.3.2 of (2). Eq. 7.3.1 and Eq. 7.3.2 of (2) can be rewritten as,

$$\begin{aligned} \int_{0}^{z} x^{-\frac{1}{2}} \cos(x)dx &= \sqrt{2\pi}\, C\left(\sqrt{\frac{2z}{\pi}}\right) \\ \int_{0}^{z} x^{-\frac{1}{2}} \sin(x)dx &= \sqrt{2\pi}\, S\left(\sqrt{\frac{2z}{\pi}}\right) \end{aligned} \tag{A.17}$$

For $n = 1$, we can solve I_0 using (A.15) as,

$$I_0 = \mathcal{I}_1\left(\sqrt{\frac{2z}{\pi}}\right) - \mathcal{I}_1\left(\sqrt{\frac{2z_0}{\pi}}\right) \tag{A.18}$$

where $\mathcal{I}_1(y)$ is defined as,

$$\mathcal{I}_1(y) = y^{\frac{1}{2}} \sin(y-\phi) - \sqrt{\frac{\pi}{2}}\left[\cos(\phi)S(y) - \sin(\phi)C(y)\right] \tag{A.19}$$

and for $n = 2$ case,

$$I_0 = \mathcal{I}_2\left(\sqrt{\frac{2z}{\pi}}\right) - \mathcal{I}_2\left(\sqrt{\frac{2z_0}{\pi}}\right) \tag{A.20}$$

where $\mathcal{I}_2(y)$ is defined as,

$$\mathcal{I}_2(y) = y^{\frac{3}{2}} \sin(y-\phi) + \frac{3}{2}y^{\frac{1}{2}} \cos(y-\phi) - \frac{3}{2}\sqrt{\frac{\pi}{2}}\left[\cos(\phi)C(y) + \sin(\phi)S(y)\right] \tag{A.21}$$

[2]We can compute p's and q's as follows: $p_0 = 1$, $q_{2m+1} = p_{2m}\frac{\mu-(4m+1)^2}{8(2m+1)}$, $p_{2m} = q_{2m-1}\frac{\mu-(4m-1)^2}{16m}$

For solving (A.18) and (A.20), we need to solve for Fresnel integrations. We can express $C(z)$ and $S(z)$ as, Eq. 7.3.9 and Eq. 7.3.10 of (2),

$$\begin{aligned} C(z) &= \frac{1}{2} + f(z)\sin\left(\frac{\pi}{2}z^2\right) - g(z)\cos\left(\frac{\pi}{2}z^2\right) \\ S(z) &= \frac{1}{2} - f(z)\sin\left(\frac{\pi}{2}z^2\right) - g(z)\cos\left(\frac{\pi}{2}z^2\right) \end{aligned} \tag{A.22}$$

where $f(z)$ and $g(z)$ are defined by, Eq. 7.3.27 and Eq. 7.3.28 of (2),[3]

$$\begin{aligned} \pi z f(z) &\sim 1 + \sum_{m=1}^{\infty} (-1)^m \frac{1.3\ldots(4m-1)}{(\pi z^2)^{2m}} \\ \pi z g(z) &\sim \sum_{m=0}^{\infty} (-1)^m \frac{1.3\ldots(4m+1)}{(\pi z^2)^{2m+1}} \end{aligned} \tag{A.23}$$

The values of $\mathcal{J}_\nu^n(z)$ using this technique are validated with Mathematica Software, (35).

[3] As we are assuming that we have large argument of z, hence we can use asymptotic expansions of $f(z)$ and $g(z)$.

BIBLIOGRAPHY

[1] M. Abramowitz and I. A. Stegun, *Handbook of Mathematical Functions with Formulas, Graphs and Mathematical Tables*, 9th printing, Dover, New York, 1970.

[2] R. Albanese and G. Rubinacci, Finite Element Methods for the Solution of 3D Eddy Current Problems, In: Advances in Imageing and Electron Physics 102, Academic Press, 1998, p. 1-86.

[3] R. Albanese and G. Rubinacci, "Integral Formulation for 3D Eddy-Current Computation using Edge Elements," IEE Proc. A 135, p. 457, 1988.

[4] R. Albanese and G. Rubinacci, "Solution of Three Dimensional Eddy Current Problems by Integral and Differential Methods," IEEE Trans. Magn. 24, p. 98, 1998.

[5] A. Banos, Dipole Radiation in the Presence of a Conducting Half-Space, Pergamon Press, Oxford, p. 135, 1966.

[6] A. Bossavit, Computational Electromagnetism, Academic Press, Boston, p. 125, 1998.

[7] J. R. Bowler, "Modelling of Eddy Current Array Sensor Sensitivities, Phase II," Technical Report for Air Force Contract Number F33615-97-D-5271, Subcontract Number 02-S437-031-C1, CNDE, Iowa State University, Oct. 31st 2002.

[8] J. R. Bowler, "Modelling of Eddy Current Array Sensor Sensitivities," Technical Report for Air Force Contract Number F33615-97-D-5271, Subcontract Number 01-S437-002-37-C1, CNDE, Iowa State University, Aug. 27th 2001.

[9] J. R. Bowler, "The Calculation of Eddy Current Distribution Using Tensor Green's Functions," Final Report for The Defense Research Agency, Farnborough, Contract Number ER1/9/4/2064/115 XR/STR, 1st November 1988 - 23rd June 1994.

[10] J. R. Bowler, S. A. Jenkins, H. A. Sabbagh and L. D. Sabbagh, "Eddy-Current probe impedance due to a volumetric flaw," J. Appl. Phys. 70, No. 3, p. 1107, 1991.

[11] J. R. Bowler, "Eddy Current Calculations Using Half-Space Green's Functions", J. Appl. Phys. 61, p. 839, 1987.

[12] S. K. Burke, "A Benchmark Problem fro the Computation of ΔZ in Eddy Current Nondestructive Evaluation," J. Nondest. Eval. 7, p. 35, 1988.

[13] C.V Dodd and W. E. Deeds, "Analytical Solutions to Eddy Current Probe-Coil Problems," J. Appl. Phys., 39, p. 2829, 1968.

[14] H. Exton, Multiple Hypergeometric Functions and Applications, Series: Mathematics and its Applications, Ellis Horwood Ltd., p. 13, Chichester, 1976.

[15] H. Exton, Handbook of Hypergeometric Integrals, Theory, Applications, Tables, Computer Programs, Series: Mathematics and its Applications, Ellis Horwood Ltd., p. 13, Chichester, 1978.

[16] L. R. Foulds, *Graph Theory Applications*, Springer-Verlag, New York, p. 64, 1992.

[17] G. Gasper and M. Rahman, Basic Hypergeometric Series, Encyclopedia of Mathematics and its Applications 35, Cambridge, Cambridge University Press, p. 4, 1990.

[18] I. S. Gradshteyn and I. M. Ryzhik, *Tables of Integrals Series and Products*, 4th ed., Academic Press, New York, 1965.

[19] F. Harary, *Graph Theory*, Narosa Publishing House, New Delhi, p. 32, 1996.

[20] R. D. Graglia, D. R. Wilton and A. F. Peterson, "Higher Order Interpolatory Vector Bases for Computational Electromagnetics," IEEE Trans. Ant. Prop. 45, p. 329, 1997.

[21] H. W. Hale, "A Logic for Identifying the Trees of a Graph," Trans. AIEE PAS-80, p. 195, 1961.

[22] R. F. Harrington, Field Computation by Moment Methods, Macmillan, New York, 1968.

[23] R. F. Harrington, Time Harmonic Electromagnetic Fields, McGraw-Hill, New York, 1961.

[24] J. Jin, The Finite Element Method in Electromagnetics, Wiley, New York, 1993, p. 231.

[25] E. Kreyszig, Advance Engineering Mathematics, 8th ed., Wiley, 1999.

[26] S. W. Lee, J. Boersma, C. L. Law and G. A. Deschamps, "Singularity in Green's Function and Its Numerical Evaluation," IEEE Trans. Ant. Prop. AP-28, p. 331, 1980.

[27] D. McA. McKirdy, S. Cochran, G. B. Donaldson and A. McNab, Theoretical Consideration of Fatigue Crack Detection and Characterisation Using SQUID Sensors, In: R Collins W D Dover J R Bowler and K Miya (eds.), Nondestructive Testing of Materials. IOS Press, Amsterdam, 1995, p. 185.

[28] P. Morse and H. Feshbach, Methods of Theoretical Physics, McGraw-Hill, New York, 1953, p. 1263.

[29] W. H. Press, B. P. Flannery, S. A. Teukolsky and W. T. Vetterling, *Numerical Recipes in Fortran, The Art of Scientific Computing*, Cambridge, Cambridge University Press, 1992.

[30] G. Rubinacci and A. Tamburrino, "Edge Elements Based Numerical Computation of Dipole Density in ECT Problems," Draft Performace Report for UCT/AFML, Project Number 404-25-24, Daeimi, July 30 2002.

[31] D. H. Schaubert, D. R. Wilton and A. W. Glisson, "A Tetrahedral Modeling Method for Electromagnetic Scattering by Arbitrarily Shaped Inhomogeneous Dielectric Bodies," IEEE Trans. Ant. Prop. AP-32, p. 77, 1984.

[32] D. Sun, J. Manges and X. Yuan, "Spurious Modes in Finite-Element Methods," IEEE Ant. Prop. Mag. 37, p. 12, 1995.

[33] C. T. Tai, Dyadic Green Functions in Electromagnetic Theory, 2nd ed., IEEE Press, New York, 1993, p. 55

[34] J. S. van Welij, "Calculation of Eddy Currents in Terms of H on Hexahedra," IEEE Trans. Magn. 21, p. 2239, 1985.

[35] Wolfram Research Inc., "Mathematica Software," Version Number 4.1.0.0.

[36] A. D. Yaghjian, "Electric Dyadic Green's Function in the Source Region," IEEE Proc. 68, p. 248, 1980.

ACKNOWLEDGEMENTS

I would like to take this opportunity to express my thanks to those who helped me with various aspects of conducting research and the writing of this thesis. First and foremost, Dr. John R. Bowler for his guidance, patience and support throughout this research and the writing of this thesis. His inspirational teaching style, insights and words of encouragement have often inspired me and renewed my hopes for completing my graduate education. I would also like to thank my committee members for their efforts and contributions to this work: Dr. Gary Tuttle and Dr. R. Bruce Thompson. I would also to thank Dr. G. Rubinacci and Dr. A. Tamburrino for their contribution in the development of the theoretical aspects of the theory. I would also take this opportunity to thank Dr. C. P. Chiou for conducting the experimental part of the project. I would additionally like to thank Dr. N. Bowler for her guidance throughout the initial stages of my graduate career. Last but not least, I would like to thank all my colleagues and friends for their support and encouragement.

This work was carried out under Air Force Research Laboratory, Materials and Manufacturing Directorate, Nondestructive Evaluation Branch Contract F33615-97-D-5271, Delivery Order 031 with Universal Technology Corporation as prime contractor. The Air Force Program Manager was John H. Barnes, AFRL/MLLP. The subcontract 02-S437-031-C1 was carried out by Iowa State University, Center for Nondestructive Evaluation.